Available online at www.sciencedirect.com
ScienceDirect
Tectonophysics 426 (2006) 7–30
TECTONOPHYSICS
www.elsevier.com/locate/tecto

Seismicity, deformation and seismic hazard in the western rift of Corinth: New insights from the Corinth Rift Laboratory (CRL)

P. Bernard [a,*], H. Lyon-Caen [b], P. Briole [a], A. Deschamps [h], F. Boudin [a], K. Makropoulos [d], P. Papadimitriou [d], F. Lemeille [c], G. Patau [a], H. Billiris [e], D. Paradissis [e], K. Papazissi [e], H. Castarède [a], O. Charade [a], A. Nercessian [a], A. Avallone [a], F. Pacchiani [b], J. Zahradnik [f], S. Sacks [g], A. Linde [g]

[a] *Institut de Physique du Globe de Paris, France*
[b] *Ecole Normale Supérieure de Paris, France*
[c] *Institut de Radioprotection et de Sûreté Nucléaire, France*
[d] *University of Athens, Greece*
[e] *Technical University of Athens, Greece*
[f] *Charles University, Prague, Czech Republic*
[g] *Carnegie Institution of Washington, United States*
[h] *Université de Nice-Sophia Antipolis, France*

Received 3 March 2004; accepted 7 February 2006
Available online 10 August 2006

Abstract

This paper presents the main recent results obtained by the seismological and geophysical monitoring arrays in operation in the rift of Corinth, Greece. The Corinth Rift Laboratory (CRL) is set up near the western end of the rift, where instrumental seismicity and strain rate is highest. The seismicity is clustered between 5 and 10 km, defining an active layer, gently dipping north, on which the main normal faults, mostly dipping north, are rooting. It may be interpreted as a detachment zone, possibly related to the Phyllade thrust nappe. Young, active normal faults connecting the Aigion to the Psathopyrgos faults seem to control the spatial distribution of the microseismicity. This seismic activity is interpreted as a seismic creep from GPS measurements, which shows evidence for fast continuous slip on the deepest part on the detachment zone. Offshore, either the shallowest part of the faults is creeping, or the strain is relaxed in the shallow sediments, as inferred from the large NS strain gradient reported by GPS. The predicted subsidence of the central part of the rift is well fitted by the new continuous GPS measurements. The location of shallow earthquakes (between 5 and 3.5 km in depth) recorded on the on-shore Helike and Aigion faults are compatible with 50° and 60° mean dip angles, respectively. The offshore faults also show indirect evidence for high dip angles. This strongly differs from the low dip values reported for active faults more to the east of the rift, suggesting a significant structural or rheological change, possibly related to the hypothetical presence of the Phyllade nappe. Large seismic swarms, lasting weeks to months, seem to activate recent synrift as well as pre-rift faults. Most of the faults of the investigated area are in their latest part of cycle, so that the probability of at least one moderate to large earthquake ($M=6$ to 6.7) is very high within a few decades. Furthermore, the region west to Aigion is likely to be in an accelerated state of extension, possibly 2 to 3 times its mean interseismic value. High resolution strain measurement, with a borehole dilatometer and long base hydrostatic tiltmeters, started end of 2002. A transient strain has

* Corresponding author. Tel.: +33 1 44 27 24 14.
E-mail address: bernard@ipgp.jussieu.fr (P. Bernard).

0040-1951/$ - see front matter
doi:10.1016/j.tecto.2006.02.012

been recorded by the dilatometer, lasting one hour, coincident with a local magnitude 3.7 earthquake. It is most probably associated with a slow slip event of magnitude around 5±0.5. The pore pressure data from the 1 km deep AIG10 borehole, crossing the Aigion fault at depth, shows a 1 MPa overpressure and a large sensitivity to crustal strain changes.

Keywords: Seismicity; Gulf of Corinth; Deformation; Seismic Hazard; Normal faulting; Rifting

1. Introduction

The rift of Corinth in Greece has been long identified as a site of major importance for earthquake studies in Europe, producing one of the highest seismic activities in the Euro-Mediterranean region: 5 earthquakes of magnitude greater than 5.8 in the last 35 years, 1 to 1.5 cm/year of north–south extension, frequent seismic swarms, and destructive historical earthquakes (Jackson et al., 1982; Makropoulos et al., 1989; Rigo et al., 1996; Papazachos and Papazachou, 1997; Clarke et al., 1997; Briole et al., 2000; Hatzfeld et al., 2000). It appears as an asymmetrical rift, the most active normal faults dipping north, resulting in the long term subsidence of the northern coast, and on the upward displacement of the main footwalls (Armijo et al., 1996). The latter is superimposed on the general uplift of the northern Pelopponesus. The stratigraphy reflects the present and quaternary tectonics of the rift: to the north of the gulf, the mountainous, subsiding Hellenides limestone nappes are outcropping almost everywhere, whereas to the south, these nappes are mostly covered by a thick (several hundreds of meters) conglomerate layer, and only outcrop on the footwall of the southern active faults (e.g., Armijo et al., 1996; Ghisetti and Vezzani, 2004). Near the sea, and offshore, on the hanging walls of the normal faults, the conglomerates are covered by finer, recent deposits (sands and clay), up to 150 m thick in the Aigion harbour (Pitilakis et al., 2004; Cornet et al., 2004b).

The recent large earthquakes of the central part of the rift (Eratine of Phokida, M=6.3, 1965; Antikyra, M=6.2, 1970; Galaxidi, M=5.8, 1992, Aigion, M=6.2, 1995) all activated offshore faults and present shallow north-dipping nodal planes (Baker et al., 1997). These planes are shown to be the fault planes at least for the 1995 and probably for the 1992 earthquakes (Hatzfeld et al., 1996; Bernard et al., 1997). These 30° to 35° dip angles significantly differ from the 45° to 50° dip angle of the three earthquakes of the Corinth, 1981 sequence (Jackson et al., 1982), at the eastern end of the rift, implying different rheological and/or structural conditions.

Since the occurrence of the destructive Galaxidi 1992 and Aigion 1995 earthquakes, the rift became the target for a large international effort on earthquake research, mostly at the European level, leading in the last few years to the development of the Corinth Rift Laboratory (CRL) project, concentrated in the western part of the rift, around the city of Aigion. (Cornet et al., 2001, 2004a; WEB: http://www.corinth-rift-lab.org).

CRL is devoted to observe and model the short and long term mechanics of the normal fault system. The target area, about 30×30 km^2, was selected in the western part of the rift for several reasons: (1), the local strain rate, larger than 10^{-6}, and the microseismic activity are highest; (2), this area does not count any source of destructive (M>5.5) earthquake since about one century. The previous two local events hitting the city of Aigion occurred in 1817 and 1888, with an estimated magnitude of around 6; (3), it is located at the western limit of the 1995 Aigion earthquake rupture area, M=6.2 (Bernard et al., 1997), which did not occur on the Aigion fault but on an offshore fault to its E-NE; and (4), the gulf is narrowest there, allowing mostly on-land field and instrumental studies.

Focussed tectonic studies in this area have produced detailed maps of the main presently active faults, and assessed their seismic activity through morphological studies, trenching through fault scarps with dating of paleoearthquakes, and study of uplifted marine terraces (Pantosti et al., 2004a,b). Independently of CRL, offshore faults were recently mapped with high resolution bathymetry by the Hellenic Center of Marine Research (Sakellariou et al., 2003).

The selected area is a place where not only one may expect a moderate to large earthquake (M>6) to occur in the coming decades, but also where various transient deformation processes are expected to occur frequently, as evidenced by the commonly reported earthquake swarms. These might be accompanied by large amplitude creep on faults, as has been first reported by Linde et al. (1996) for the shallow creeping section of the San Andreas fault. The instrumentation is therefore also aimed at a better understanding of the cross-triggering between aseismic creep, fluid flow, and earthquakes activity on faults (e.g., Bernard, 2001). In complement to these studies on mechanical processes, the gathered data, complemented by temporary field experiments, are also used for detailed travel-time and reflection-tomography, revealing a strongly heterogeneous structure of the shallow and upper crust (Latorre et al., 2004).

A major, medium-term target of CRL is the drilling of a deep borehole (>4 km) for the installation of a deep geophysical observatory within and near a fault zone, at seismogenic depth, for investigating in particular the role of fluids transients in the mechanical behaviour of faults, and their coupling with seismicity.

The aim of the paper is to present the scientific and technical achievements of the new monitoring arrays for seismicity and strain. We first briefly review the instrumentation effort in the rift of Corinth since a decade. We then present in more detail the results from the seismic arrays monitoring the local seismicity, the repeated and continuous GPS, and the high-resolution strain and tilt measurements. This allows a detailed discussion on the geometry and tectonic loading of the various active faults, and on the seismic hazard of the area.

2. The geophysical monitoring arrays in the rift of Corinth

Several arrays have been installed in this area for continuous monitoring of the seismicity (Fig. 1). Until 2000, monitoring the local seismicity was mostly achieved by the CORNET array of the University of Athens (NKUA) and by the PATNET array of the University of Patras, but the target area is located on the edge of both arrays, providing poorly constrained hypocentral locations. Since then, a new seismic network, CRLNET was provided by French CNRS to focus on the CRL target (Lyon-Caen et al., 2004).

CRLNET is made up of 12 recording stations equipped with 2 Hz velocimeters: 7 are installed on the southern coast of the gulf and 5 on the northern coast. Its primary focus is on the Aigion and Helike fault activity, justifying its narrow EW extension (15 km). In order to properly monitor small magnitude events, velocimeters from the 7 southern stations were installed in 60–130 m deep boreholes in order to avoid very soft soils and human activity noise which is quite large in the Aigion plain. However only at the southern-most site

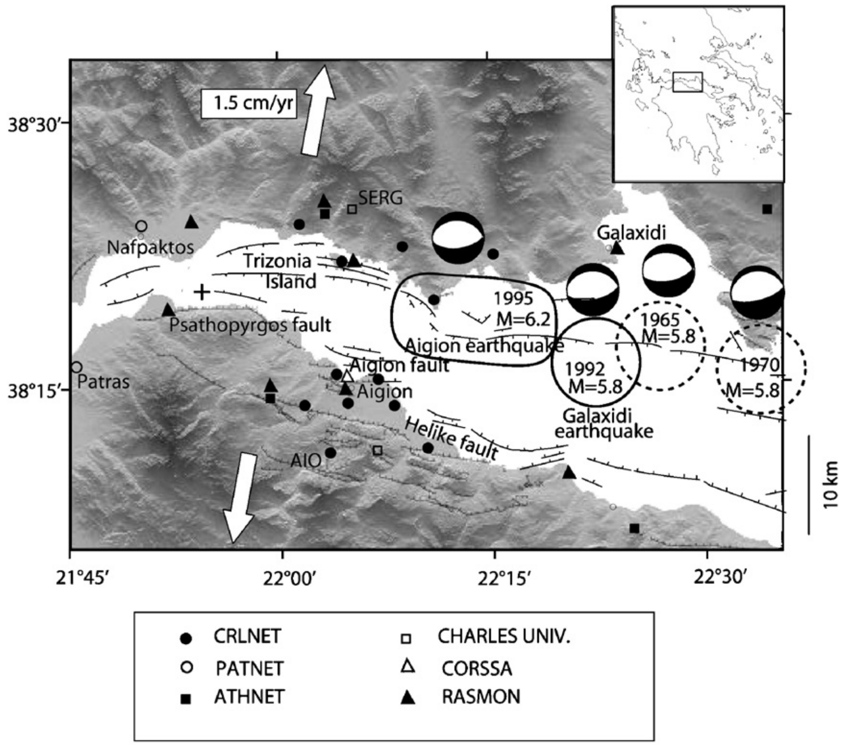

Fig. 1. Seismological arrays in the western rift of Corinth. The cross is for the 3rd December 2002 earthquake. Focal mechanisms from Baker et al. (1997), Hatzfeld et al. (1996), and Bernard et al. (1997). Solid and dashed lines: estimated area of seismic ruptures. Offshore faults from Moretti et al. (2003). Cross: epicentre of the 3rd December 2002 earthquake.

(AIO), the seismometer could be installed directly on the limestone. The signal, sampled at 125 points/s, is recorded continuously by TITAN3NT recorders. Data are stored on site and regularly gathered and sent to IPGP in Paris and to NKUA in Athens. These 12 stations are complemented by 2 stations from ATHNET run by the University of Athens. We also integrate in our dataset observations made at one broad-band station (SERG) by the Prague University in collaboration with the Patras University (Zahradnik, 2003).

Strong motion accelerometers were first installed on bedrock, since 1993 (RASMON array, University of Athens). In 2002, a borehole accelerometer array, CORSSA, has been installed in the soft soil of the Aigion harbour, down to 180 m in depth, for studying the non linear response of soils (Pitilakis et al., 2004). It was initiated by the CORSEIS E.C. project, under the responsibility of the University of Thessaloniki (AUTH), NKUA, and IRSN. Independently of CRL, the Charles University of Prague has installed 2 broad-band seismometers and two accelerometers in the target area, in 1999, in collaboration with the University of Patras.

In addition, several arrays have been installed for measuring strain and strain-related processes (Fig. 2). Based on the knowledge of strain gradients from yearly repeated measurements since 1990 (Briole et al., 2000), five continuous GPS have been installed, covering the area, and centered on the Trizonia island: this array geometry allows to have access to NS and EW gradients of the strain rate, thus across the rift as well as along the trend of the fault system. In 1995, tiltmeters and strainmeters (silicium *Blum* type) were installed in the Galaxidi cave, on the northern coast of the Gulf, 50 km ENE to Aigion, and were used to constrain the source of the VAN electrical "precursor" of the 1995 Aigion earthquake (Pinettes et al., 1998). This experiment however stopped in 1999, because of the rather high thermal perturbations and local mechanical instabilities in the cave, and because the site was too far from the CRL target area. In 1997, borehole tiltmeters were installed in shallow (10 m) boreholes along the northern coast (Bernard et al., 2000; Bernard and Boudin, 2001). These instruments were also stopped in 2002, due to insufficient resolution, step-like response to seismic waves, and drift outside the measurement range. More suitable installations were then achieved: one borehole *Sacks-Evertson* dilatometer was installed in 2002 at 150 m in depth, in Trizonia, and, less than 1 km away, a

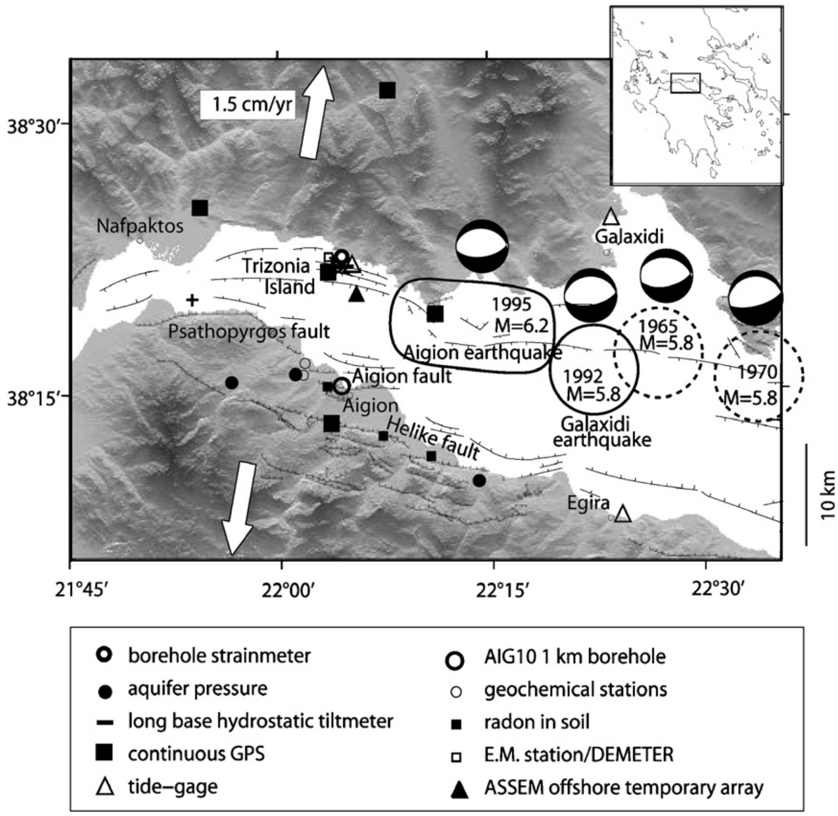

Fig. 2. Strain-related monitoring arrays. Same seismotectonic information as in Fig. 1.

high-resolution, long base hydrostatic tiltmeter was installed at 3 m in depth (Bernard et al., 2004). The external strain sources (sea level and air pressure) are controlled with tide-gages (near Galaxidi, in Trizonia, and on the southern coast near Egira, 50 km east to Aigion) and barometers (near Aigion). The Galaxidi and Egira tide-gages, although remote from the target area, are kept in operation for detecting and modeling eigen-modes of oscillation, sea-tide, and possibly tsunami propagation in the Gulf, which all influence the high resolution strain records.

To complement these direct measurement of strain, pressiometers and flowmeters are installed in existing boreholes reaching confined aquifers, on the southern coast, acting as strain-gages (Léonardi and Gavrilenko, 2004). The 1 km deep borehole drilled in the Aigion harbour, AIG10, cutting the Aigion fault at 750 m in depth (DGLab-Corinth E.C. project), and reaching an aquifer confined in the footwall, is also presently monitored with a piezometer (Cornet et al., 2004b).

Other installations were aimed at tracking underground gas or fluid flow transient anomalies through the near-surface fault systems, in relationship with deep strain or fluid transients: Radon probes were installed since 1997 in soil on the Helike and the Aigion fault scarps, and in karstic springs (Bernard et al., 2000). Geochemical monitoring systems were installed since 2001 on artesian wells selected for their contamination from in-flow from deep aquifers (Pizzino et al., 2004).

Finally, a permanent electromagnetic station has been installed in 2004 in the Trizonia island, recording two horizontal components of the electric field and three

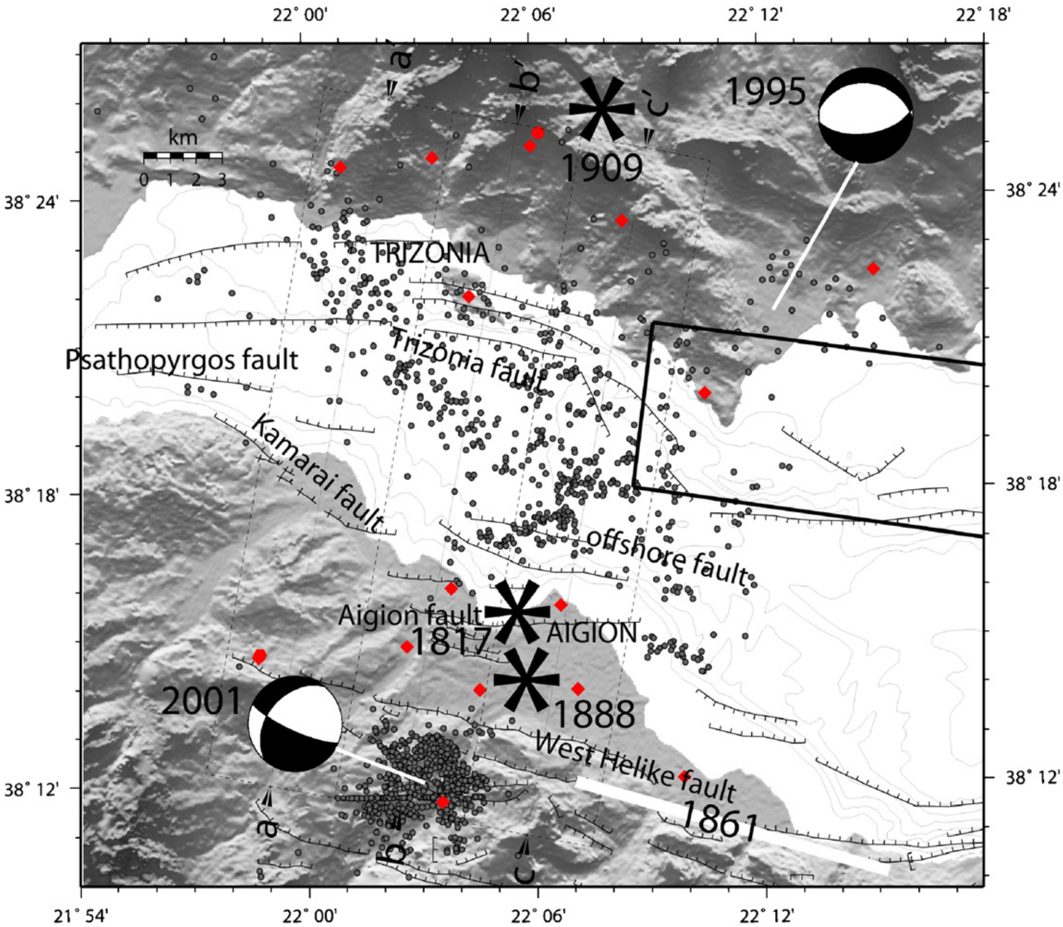

Fig. 3. Map view of the 2000–2001 seismicity. Truncated rectangle to the east corresponds to the 1995 rupture area, from Bernard et al. (1997). Stars correspond to center of maximal intensity of historical earthquakes, from Papazachos and Papazachou (1997), and Ambraseys and Jackson (1990). Straight white segment indicates dimension of the reported surface rupture of the Helike 1861 earthquake (Papazachos and Papazachou, 1997). Faults from Moretti et al. (2003). Bathymetry is produced by HCMR (Alexandri et al., 2003). Focal mechanism is for the 1995 earthquake and the mainshock of the 2001 swarm. Dotted lines: cross-sections presented in Fig. 4.

components of the magnetic field, in the ULF and ELF-VLF frequency bands (Zlotnicki et al., 2005). This station is the ground segment of the DEMETER satellite from *Centre National d' Etudes Spatiales* (CNES), launched in 2004, for monitoring the electromagnetic signals related to earthquake and volcanic activity.

3. CRLNET: seismic activity and fault geometries at depth

The main characteristics of the microseismicity of the western rift of Corinth is a strong clustering between 5 and 10 km, presenting a gentle slope towards north, as was first revealed by a temporary experiment in 1991 (Rigo et al., 1996). These authors interpreted it as a detachment zone, on which the major north-dipping normal faults are rooting, and which acts as a shear zone controlling the fault pattern of the rift. With a denser array and a longer period of monitoring, CRLNET now allows a better localization and characterization of the active portions of the faults in the target area, and the identification and detailed analysis of swarms.

Fig. 3 presents 2 years of seismicity located with CRLNET data using the 1D velocity model of Rigo et al. (1996) and Hypo71 software. Over 6000 events have been recorded but only about 2000 events are precisely located, mostly within the area covered by the array. Events with at least 5 P and 4 S phase readings, standard location errors smaller than 1 km in all directions and rms smaller than 0.1 s were retained. Various tests, including velocity structure perturbations and initial depth and location perturbations were performed. They indicate that the uncertainty is less than 1 km in all directions for events inside the network.

The largest swarm of the past 4 years occurred in spring 2001, at the southern limit of the array (see bottom of Fig. 3), culminating with a main shock with magnitude Ml = 4.3, and tens of earthquakes with Ml > 3.0 (Lyon-Caen et al., 2004; Zahradnik et al., 2004). Relocations and multiplet analysis for this swarm revealed the slip of a NW dipping fault, reactivated in the present NS extension as a normal faulting with a large right-lateral strike-slip component (Pacchiani et al., 2003) (see the focal mechanism in Fig. 3). This fault appears distinct from the more northern, EW striking Corinth rift normal fault system.

More to the north, below the Gulf, the seismicity presents a similar image to that of the 1991 experiment (Rigo et al., 1996) (Fig. 4): the shallow dip of the seismic cloud towards north is clearly confirmed. The subhorizontal seismicity band is presented in Fig. 4 by the vertical cross-sections *aa′, bb′* and *cc′* of Fig. 3, in a direction parallel to the mean extension of the rift, which is also perpendicular to the strike of the western Helike fault. It appears about 2 to 2.5 km thick, but may be thinner, as the hypocentral depth errors could broaden the structure by up to about 1 km.

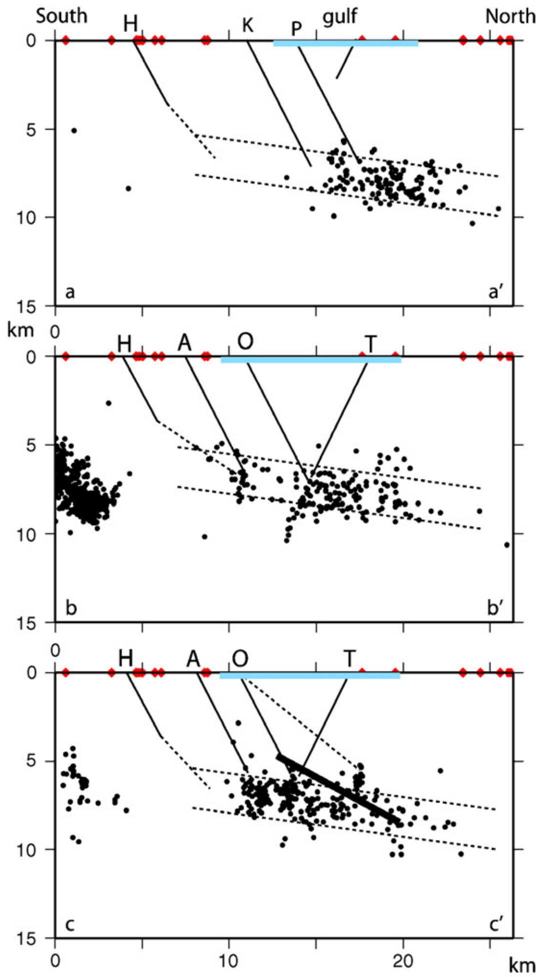

Fig. 4. Vertical, N10° E cross-sections of the 2000–2001 seismicity on profiles *aa′*, *bb′*, *cc′* of Fig. 3. Faults are assumed with large dip angle (60°): Aigion (A), Helike (H) faults, Kamarai (K), Psathopyrgos (P) faults, (O), offshore, and (T), Trizonia faults. A small dip offshore fault (O) is represented with a dotted line on profile *cc′*. The thick segment is the fault plane of the 1995 Aigion earthquake. Horizontal grey layer near the surface indicates the gulf location. The parallel, dotted lines dipping gently north outline the boundaries of the creeping, seismic layer.

To the south-east, near the city of Aigion, the microseismicity gets closer to the surface, with about 10 earthquakes at 5 km in depth and shallower, beneath the southern coast. The shallowest event is at 3.5 km in depth (eastern section *cc′*), located right on the Aigion fault if the latter keeps the 60° dip angle observed for the first kilometer (constrained by the AIG10 borehole, see Cornet et al., 2004b). Other shallow events, around 5 km in depth, are significantly south (2 km) to the Aigion fault, within its footwall (section *bb′*), and may thus be related to the Helike fault. The Aigion and the central part of the West Helike faults are thus relatively well constrained, from the surface down to a depth of about 6 km where they enter in the highly seismic layer and possibly join each other.

To the north, this layer is affected by the rooting of more northern faults, as seen on Fig. 3: the offshore fault north to Aigion (O), the Psathopyrgos fault (P), and the *en echelon* Kamarai fault system (K) connecting the latter to the Aigion fault.

The dip angle of the offshore and Kamarai faults cannot be constrained directly by the seismicity. For the dip angle of the offshore fault, north to the Aigion fault, two alternative values can be proposed: a high value, around 60°, similar to that of the Aigion fault; or a low value, 30 to 35°, similar to that of the 1995 fault plane. In the latter case, this offshore fault would be very close to the geometrical westward continuation of the 1995 rupture plane, thus implying a major, low-dip angle active fault, 30 km long. The knowledge of the dip of this fault is therefore a key question for understanding the mechanics of this part of the rift.

In the absence of direct measurements, two indirect arguments can be put forward in favour of the 60° dip angle model for the offshore fault. First, this model has the advantage to avoid the mechanical problems due to slip on two neighbouring, non-parallel fault planes (Aigion and Offshore), as large differences in dip angles implies larger strains than with parallel faults, within the crustal blocks between the faults or beneath them. This argument has also the advantage of simplicity, assuming similar mechanical conditions of the growth for both faults.

A second, more constraining argument is related to the antithetic, offshore Trizonia fault. The latter presents a 400 m high fault scarp and the current depocenter of the rift is shifted to the north, closer to this fault than to the north dipping offshore fault (Moretti et al., 2003). The Trizonia fault is thus a major active structure. A deep rooting of this fault is however not possible with a low-angle, north dipping offshore fault, as the latter would intersect the Trizonia fault at less than 3 km in depth. However, the 60° dip model allows the Trizonia fault to extend up to 6 km downdip, in better agreement with the observations above. We therefore consider a 60° dip for the north dipping offshore fault as the most likely model. The same line of arguments can be followed for the Kamarai fault system; in addition, the mechanical constraint that the latter shall not cross the offshore fault makes a low dip angle impossible. Thus, a 60° dip angle will be assumed for the Aigion, the Offshore, and the Kamarai faults.

To the south of the Kamarai and of the Pasthopyrgos faults, the western part of the West Helike fault, mapped on the western section (*aa′*), present no microseismic activity. The closest seismic cluster is 15 km north to the Helike fault scarp, and only 4 km north to the Kamarai fault system. Its connection to the Kamarai fault is thus much more likely, as it would imply a dip angle of about 60° for this fault, compatible with the dip angle of the neighbouring faults to the east. The extension of this cluster to the north would then provide evidence for the loading of the root of the Kamarai fault.

West to the 1861 Helike rupture, the West Helike fault plane appears presently inactive in terms of microseismicity. This is consistent with the geological estimates by Pantosti et al. (2004a) and by Flotté (2003) who noted that this segment is no longer active, or has an extremely low slip rate. Thus, the western Helike fault is then most probably deactivated, in its western section, by the new Kamarai fault, consistent with geological investigations.

This interpretation provides a simple explanation for the microseismic pattern of the area (see Figs. 5 and 3). The southern limit of the area with highest seismicity rate is oriented NW-SE, along a line nearly parallel to the Kamarai fault system, but shifted to the north by 5 km. A 60° dipping fault towards NNE would reach this limit at the depth of 7 km, thus coinciding to this seismicity boundary: the southern edge of the microseismicity thus marks the root of the steep Kamarai fault segment.

In summary, we hypothetize that the 60° dipping Aigion fault and the eastern part of the western Helike faults are loaded around 5–6 km in depth by continuous slip on the detachment zone, and are both subject to some seismic creep from these depths up to 4 km. To the west, the 60° dipping Kamarai fault seems to have contributed to lock the western part of the West Helike fault.

Part of the seismicity on the southern side of the Helike fault could be related to the updip continuation of the detachment layer towards south, probably reaching the now mostly inactive Mamoussia and Pirgaki faults. However, clusters such as the 2001 crisis, or as the one located at 10 km in depth beneath the center of the gulf, cannot be associated to the active normal faults reported at the surface.

In this general seismotectonic frame, the microseismicity 5 to 7 km below the northern coast (section *bb′* and *cc′*, Fig. 4) is not associated to any of the identified, outcropping major faults. For simple mechanical compatibility with the south-dipping Trizonia fault,

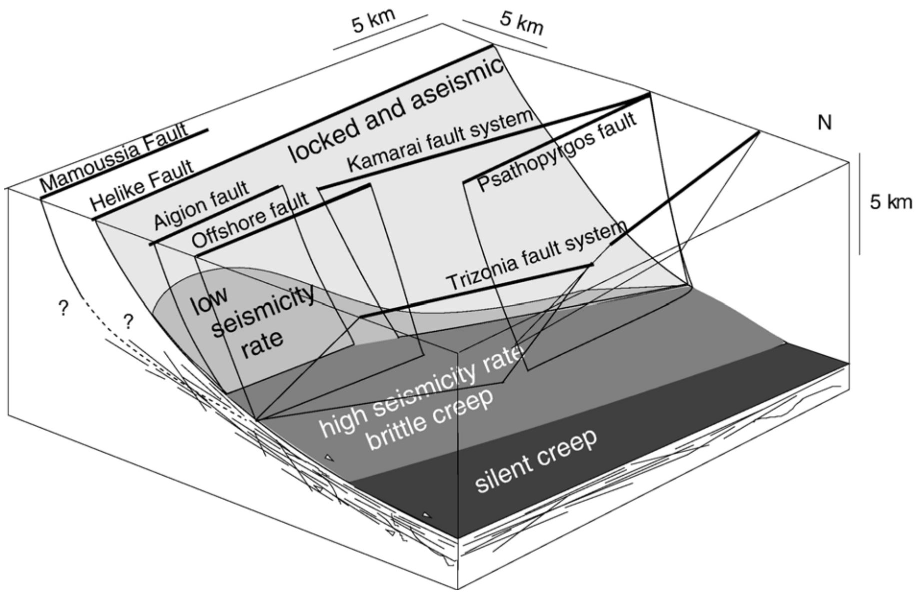

Fig. 5. Sketch of the proposed fault geometry and observed microseismic activity in 2000-2001.

one may suggest that these earthquakes are associated to south dipping, blind normal faults.

Finally, one should recall that this image represents only 2 years of seismicity, and may not represent a statistically significant hypocentral distribution representative of the seismicity of the last decades (we recall however the similar pattern obtained in 1991). Our inference on the locked state of the western West Helike fault, and on the large dip angles of the Kamarai and Psathopyrgos faults, should therefore be seen only as a plausible working hypothesis to be tested with a longer catalogue, which presently helps us to identify the targets for future, focussed studies.

4. GPS: secular and transient strain of the rift

The geodetic network deployed in and around the rift of Corinth consists of approximately 200 points The whole network covers a surface of about 100 × 80 km, which corresponds, including sea surface, to 1 point every 5 km. This dense network allows us to have a satisfactory sampling of the main active faults in the region.

Eleven field surveys on this network were achieved in 1990, 1991, 1992, 1993, 1994, June 1995, October 1995, 1997, 1999, 2000 and 2001. Two of them (1992 and June 1995) were performed for a post-seismic scope after the 1992 Galaxidi (Ms = 5.9) and the 1995 Aigion (Ms = 6.2) earthquakes. The GPS data of all the surveys carried out in the region since 1990 were processed with *GAMIT/GLOBK* software (King and Bock, 1998; Herring, 1998). The velocity field obtained from the GPS data analysis, calculated with respect to the Eurasian plate, is represented in Fig. 6. This velocity field indicates an almost N–S opening direction, and reveals two main features: firstly, an important gradient of deformation localized off-shore, on a very narrow band, in the central part of the gulf; secondly, an increase of the opening rate from east to west ranging between 11 mm/year in its central part and 16 mm/year in the west. These rate values do not take into account the earthquakes contribution. Horizontal co-seismic displacements observed for the Ms = 6.2 June 15, 1995 event reach 15 cm near the northern coast, and quickly decrease when moving away towards the north. Little deformation appears in the southern block, except in the region of the Aigion 1995 rupture, and near the western end of the rift, close to the Psathopyrgos fault.

In order to track possible temporal variations in the straining rates, such as those reported in subduction zones (e.g., Dragert et al., 2001), five permanent GPS stations were installed. The choice of the locations was aimed at constraining the strain gradients in their principal directions, related to the north–south secular extension of the rift, and to the east–west segmentation of the active normal faults, including the western limit of the 1995 rupture area. The network is operational without telemetry since June 2002. Telemetry through phone line is operational since summer 2003. The data sampled at 30 s are transmitted daily to Athens, where they are automatically processed with the GAMIT/GLOBK software. The results are made

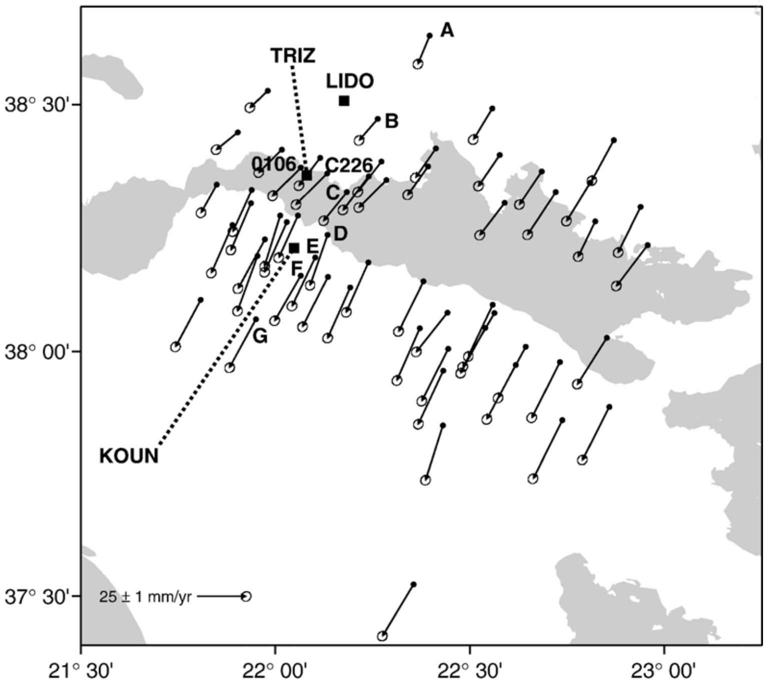

Fig. 6. Velocity field in the Gulf of Corinth obtained from the comparison of 11 years of GPS data, with a fixed Eurasia plate. Sites labelled with letters are specific sites used from the elastic modeling (Fig. 8). Solid squares are for 3 continuous GPS sites (Fig. 2). There is a clear NS velocity jump across the rift.

available on the Web site (http://geodesie.ipgp.jussieu.fr/Permanent_GPS_Corinth.htm) at IPGP.

Despite the long and frequent periods of missing data (power and/or phone failure), the time series already shows a trend compatible with that obtained from the repeated GPS campaigns (Fig. 7, bottom). No temporal change of deformation rate is observed, but the missing record periods do not allow yet a proper analysis of such effects.

We attempted to model the steady-state strain with a simple elastic model consisting of a set faults slipping at a constant rate, adjusted to the fault model adopted above. This steady-state strain is provided by the 11 years of GPS measurements, corrected from the co-seismic deformation due to the Ms = 6.2 June 15, 1995 Aigion earthquake (Avallone et al., 2004). We used the elastic homogeneous half-space approximation (Okada, 1992), considering planar fault segments with constant dislocation rates. We consider a simplified model of the rift in which the possibly creeping normal faults are invariant along the rift trend, N105° E, and where the horizontal slip is oriented N15°. The present, interseismic slip is assumed to be localized on six fault segments (F1 to F6) (Fig. 8A). The geometry of those segments is constrained by the location of the microseismicity and the on-land and offshore fault traces. In order to minimize the number of free parameters, we considered the following fault model.

Firstly, a semi-infinite fault segment (F1), dipping 7° north, allows for the continuous loading of the rift, imposing its total extension rate. Near its southern end, it simulates the shear strain localized within the microseismic layer. It stops when crossing the root of the offshore fault, assumed to dip 60° north. Fault segment F2 is the continuation of F1 towards south, 3 km long, stopping when crossing the 60° dipping Aigion fault plane. The bottom of the 60° dip offshore fault plane, F4, is allowed to creep a depths larger than 6 km, down to its contact with F1. This segment F4 also accounts for the Kamarai fault creep at depth. We do not consider creep on the Helike fault, as preliminary modeling tests show no need for it. We also considered the shallow parts of the offshore (F5) and of the antithetic, Trizonia (F6) faults, 2 km long from the surface: indeed, although these shallow segments present no seismic activity, they cut through or mark the boundary of the basin sediments and of the probably weaker upper limestone basement, which are likely to favour creep. The Helike fault, the shallow part of the Aigion fault, and the mid-depth part of the Trizonia and of the offshore faults are all considered to be locked. The effect of the Psathopyrgos fault (P) is not considered as it is located at more than 15 km west from the studied NS profile.

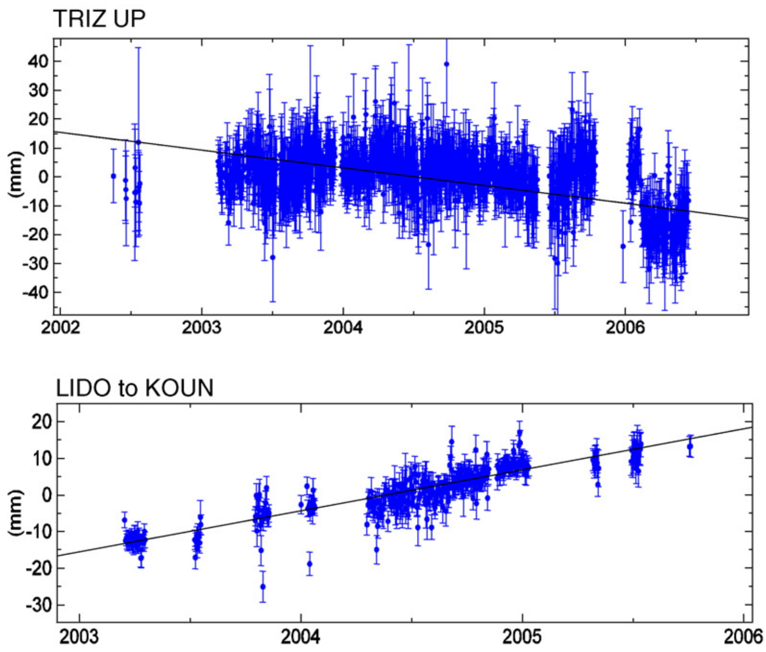

Fig. 7. *Example of displacements measured at the continuous GPS sites*. Top: vertical position at the Trizonia site (TRIZ); Bottom: horizontal distance between LIDO (northernmost station) and KOUN (southernmost station).

Several iterative inversions have been performed, with various starting models and some fixed parameters. In all cases, the slip on fault F1 is *a priori* fixed to 15 mm/year. We present here the most significative models and the associated fit (Fig. 8A). They all have a 8 mm/year slip on F4 (0 mm/year provides a reduction in fit quality).

In a first model (A), all the deep fault segment creep, and both shallow fault segments are locked. The result is a smooth NS velocity gradient, with a poor fit to the strong velocity step across the gulf. In model (B), creep at 15 mm/year on the offshore fault F5 is allowed in addition to the active faults of model A. The fit is improved. In model (C), the offshore fault F5 is creeping at higher rate of 26 mm/year, and F2 and F3 are locked. The quality of the fit is slightly improved with respect to model B: locking the bottom fault compensates the higher rate of the shallow fault. In model D, the 26 mm/year of the offshore fault F5 is reduced to 15 mm/year, and the Trizonia fault is now creeping at 5 mm/year. The model keeps the same quality of fit. Finally, model E activates all fault segments, also with a good fit to the data.

Analysing these results, one can thus reject models with no creep on the offshore shallow faults F5 and F6. There is however no resolution on the creep of the F2 and F3 faults, which can range from 0 to about 10 mm/year. The two best models are C and E, equivalent in term of fit. We prefer model E, with all faults creeping, for 3 reasons: (1), the slip rate of 26 mm/year on F5 (model C) implies a strain relaxation around this segment larger than the loading rate from the creeping segment F1. It would imply that the shallow crust is relaxing elastic strain stored in the earlier part of the seismic cycle, which poses a rheological problem, as the shallow crust is expected to relax strain quite rapidly. (2), the Trizonia fault controls the recent sedimentation, as already pointed out, and the same sediments are thus expected to be found at deeper depth on this fault than on F5. Thus, if F5 creeps at depth, then F6 should also be prone to creep at the same depth. (3), model E with an active antithetic fault F6 provides a local increase of velocity towards north for points just north to F6, which is well reproduced, at least qualitatively, by the GPS data (points C and O106).

One should note that the creep found on F5 and F6 could be reduced by considering a more adequate elastic model involving lower elastic moduli for the shallow, offshore basin (see for instance Bernard et al., 1997).

The horizontal velocity measured between the northernmost (LIDO) and southernmost (KOUN) permanent GPS sites, provides 9 mm/year of NS extension between both points. This is in excellent agreement with the prediction of all our models (see the solid squares in Fig. 8A). This also suggests that point B, only 5 km ESE to LIDO, has an anomalous, yet unexplained velocity.

We present in Fig. 8B the vertical velocities predicted by the fault models above. Globally, they all produce a

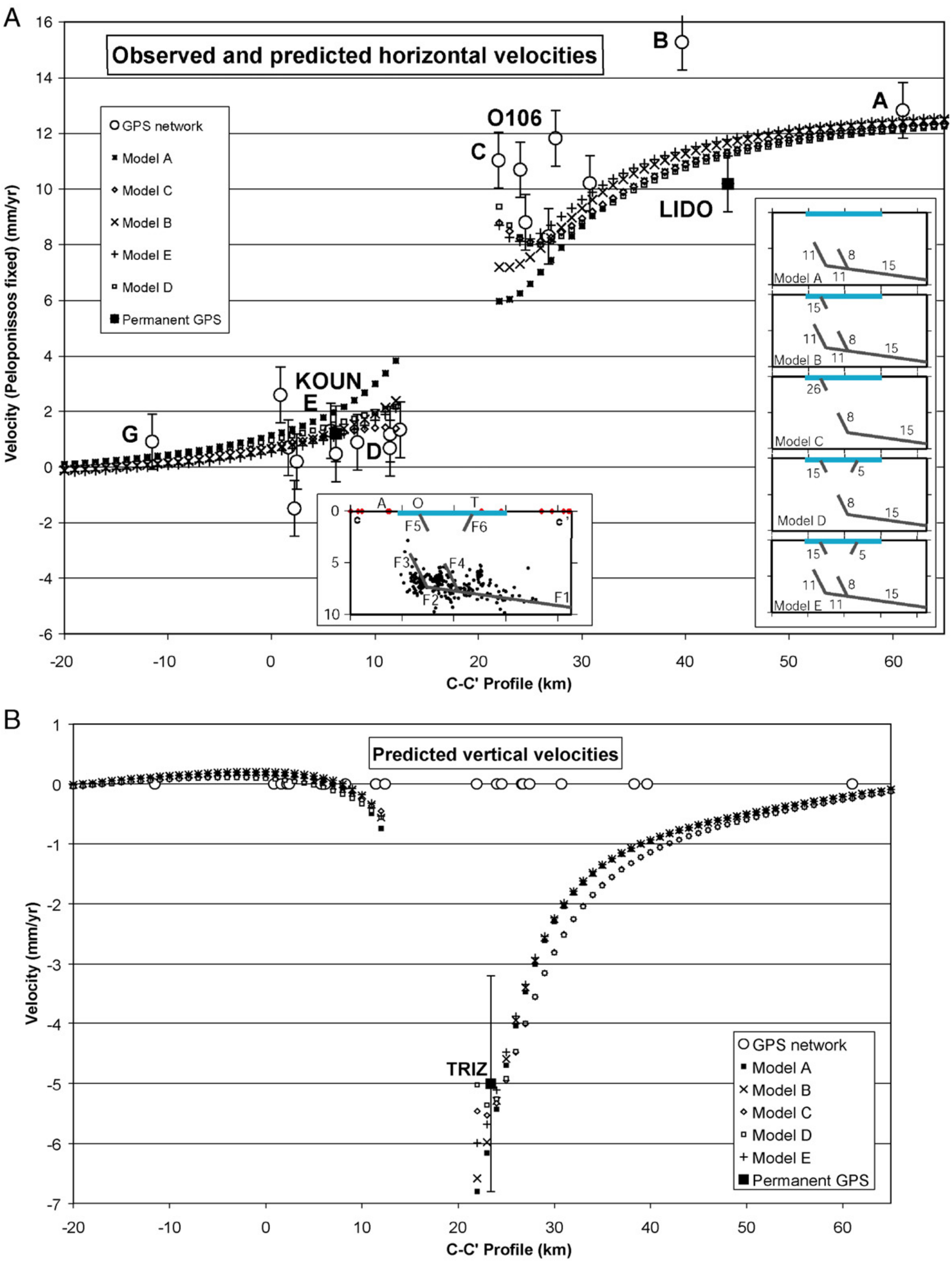

Fig. 8. (A) kinematic elastic models of the rift opening fitted to GPS and seismicity data. Circles with error bar: GPS data. Site names refer to Fig. 6. The 5 models (from A to D) are plotted with different symbols (see insert top, left). Bottom insert: position of fault segments with respect to the seismicity. Right insert: Sketch of the 5 models, with creep velocities in mm/year. Sites of the permanent GPS array (KOUN and LIDO) are represented by solid squares (KOUN is arbitrarily set at the position predicted by the models), and LIDO deduced from the data (Fig. 7, bottom). (B) predicted vertical velocities for the models of Fig. 8A. Solid square is for the measured velocity at the continuous GPS point of Trizonia (TRIZ), with a 2 mm/year uncertainty.

subsidence, with larger values near the center of the rift. The effect of a creeping F6 fault is visible on the sites nearest to it, but remains secondary. These predictions of subsidence cannot be compared to the vertical velocities measured during the repeated experiments, due to the very large uncertainties of the latter. However, they can be tested against the vertical velocity measured at the continuous GPS site of Trizonia, averaged over the last 2.5 years (Fig. 7, top). At this site, the prediction from all models is a subsidence of 5.5±0.5 mm/year, in excellent agreement with the measured one, 5±2 mm/year (solid square in Fig. 8B).

Note that these results should be taken as a first order description of the interseismic strain. First, the creeping rates might present smooth gradients along the fault dip, instead of sharp jumps. Second, part of the strain sources may not occur on single fault planes, but through unresolved distributed slip or shear within the rock body, in particular within the detachment zone and the shallow offshore crust, involving non-elastic rheology. Finally, the GPS data should be more accurately modelled in 3D, with a more realistic geometry of the active faults.

5. CRL-STRAIN: high-resolution tilt and strain monitoring

5.1. Strain records

The borehole *Sacks-Evertson* dilatometer installed in the Trizonia island is continuously recording the horizontal stress (sum of horizontal non-deviatoric components) at 150 m depth, with a resolution better than 10^{-9} (Sacks et al., 1971; Bernard et al., 2004). The dominant signal is the semi-diurnal and diurnal earth and sea tidal effects, corresponding to a few 10^{-7} strain. This signal is modulated by the mechanical effects of the free oscillations of the gulf, with eigen-mode periods ranging between 8 and 40 min. These oscillations are mostly triggered by wind and, thus, depend on its direction and strength. Their amplitude corresponds to about one centimeter of water height fluctuation. Note that these oscillations are also expected to be generated, with higher amplitudes, by offshore slumps or large shallow earthquakes, causing tsunamis to hit the shoreline at these periods.

At longer periods, days to months, the barometric pressure fluctuation acts in combination with the mean sea level variation. Both effects are not independent, as for short scale air pressure gradients, sea water may flow in or out of the gulf, and partially compensate the air pressure fluctuation, as observed from air and sea tide records (Pinettes, 1997). Finally, the rain does not produce any clear signal, implying that the water table level does not change significantly. This can be explained by the proximity of the shore line, only 30 m away, combined with the high permeability of the shallow rocks (fractured limestone).

Local, regional, and teleseismic records are well recorded by the instrument. We present in Fig. 9 the records of the 25 September 2003, M=8.1, Hokkaido earthquake, in comparison with the CMG3 velocity record at SERG, located 3 km NW. As predicted by simple theoretical analysis, the compressive stress detected by the dilatometer is approximately proportional to the horizontal ground velocity in the radial direction, with coefficients depending on the type of waves (incident P, incident SV, or Rayleigh). The Hokkaido earthquake and the related CMG3 record thus provided us the means to calibrate *in situ* the dilatometer response, taking into account the effect of the surrounding rocks up to a kilometric scale, and assuming that the sensor only responds to remote compressive strain, and not to deviatoric strain. This leads to a sensitivity of $1.09 \pm 0.16 \times 10^{11}$ D.U./strain at about 1 min period. The tidal analysis (sea and earth tide components) allows an independent calibration at about 12 h period, again assuming no sensitivity to deviatoric $1.22 \pm 0.2 \times 10^{11}$ D.U./strain, in agreement with the former calibration. However, part of the 3 m long dilatometer is surrounded by highly fractured rocks revealed by logging, and the related strong heterogeneity may produce a significant compressive response to far-field shear strain.

When looking at the long term signal on the dilatometer since its installation (Fig. 10), one

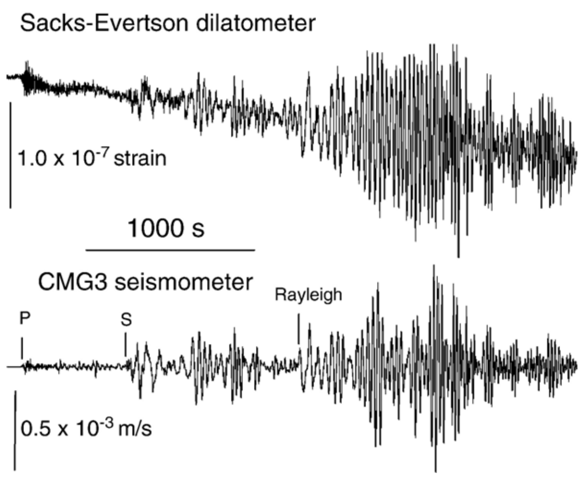

Fig. 9. Records of the 2003, 25 September, M=8.1 Hokkaido earthquake. Top: Dilatometer record in Trizonia. Bottom: CMG3 radial velocity record at SERG.

recognizes a first compressive, transient effect, lasting about 1 months, related to the stabilization of the cement and of the borehole. The more recent period shows a stable strain, with a strain rate smaller than 10^{-7}/year. The elastic interseismic strain rate predicted under Trizonia by elastic modeling is 10^{-7}/year (see paragraph 4 and Fig. 8), but the usual relaxation of the shallow crust leads us to believe that the resulting strain rate at the extensometer site should be much smaller, and hence yet unresolved.

Finally, the analysis of 30 months of continuous recording provided only one clear observation of slow transient deformation unrelated to surface perturbations, well above the noise level (Fig. 11). It started the 3rd of December 2002, around 23:00, and lasted about 1 h, with an amplitude of 1.5×10^{-7} (Bernard et al., 2004). The peak of the compression signal coincides within a couple of seconds with a Ml = 3.5 earthquake, located 14 km west. This earthquake was the largest of a seismic swarm which lasted a few weeks and produced 6 events with Ml > 3 (Catalogue of the University of Patras) (Fig. 12). The physical link between the slow and the seismic events is very likely, due to their precise time coincidence. No clear tilt signal is detected above the 10^{-7} noise level on the CMG3 broad-band record, 5 km to the north (SERG site, see Fig. 3) (Zahradnick, personal communication, 2005). Assuming the source of the strain transient to be in the vicinity of the earthquake, the equivalent minimal moment magnitude Mw of the slow event can be simply estimated from the distance and the compression step values, assuming a normal faulting slip. One finds a magnitude Mw ranging from 4.5 to 5.5, owing to uncertainties in distance and mechanism, implying that the earthquake has been only a secondary effect embedded in a much larger aseismic strain episode. Thus, although the strain transient, starting half an hour before the earthquake, can be seen as a precursor, the sequence would be better described as a unusual

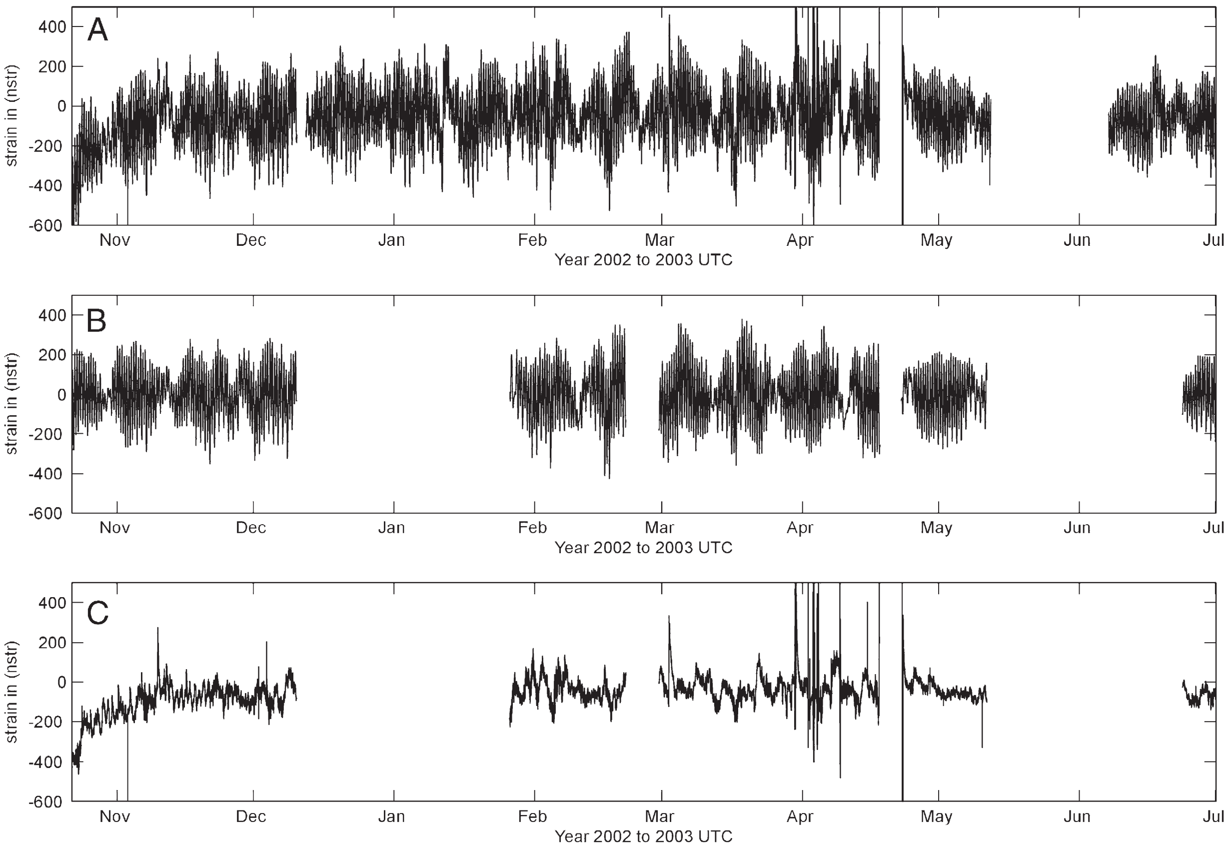

Fig. 10. Nine months of compression record at Trizonia. Top: measured compressive strain; middle: strain effect of tide and air pressure (low-pass filtered above one day), calculated with multi-linear fitting from tide and air pressure data; bottom: residual strain (tidal and air pressure effects removed). The large peaks in March and April 2003 are due to the drilling operation of a 300 m deep borehole located 30 m away.

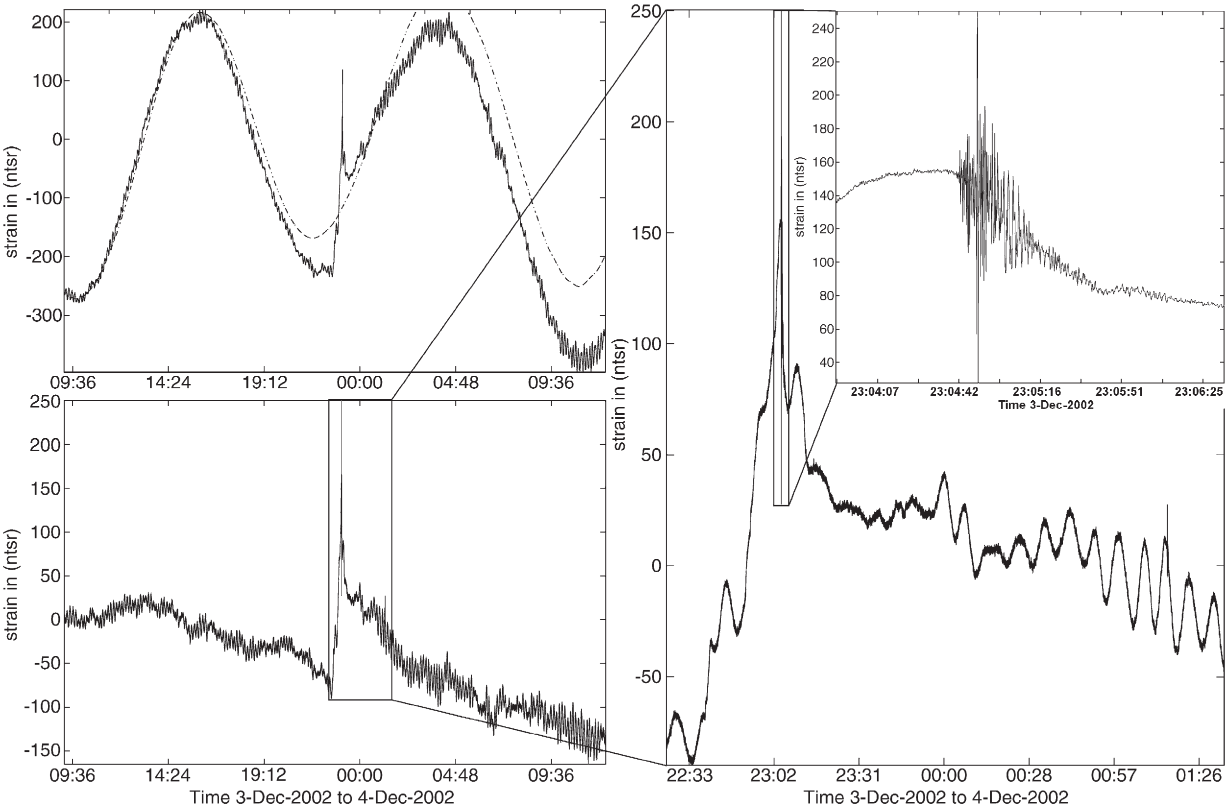

Fig. 11. Trizonia dilatometer transient record. Top left: Record of the 3rd December 2002 compression transient (amplitude 1.5×10^{-7}) superimposed on tidal wave. Dotted line: best fit model of tidal strain. Bottom left: residual when best fit models of tidal waves and air pressure are removed. Right: 3 h zoom of the transient, also showing the free oscillations of the Gulf and seismic waves of a local M=3.5 earthquake (top right insert, 150 s duration), Compression is positive. Rapid extension occurs a few seconds after the arrival of the seismic waves.

mainshock–aftershock type sequence, with a silent and slow “mainshock”.

5.2. Tilt records

About 1 km south to the dilatometer site, in the Trizonia island, two orthogonal hydrostatic tiltmeters, 15 m long, have been installed at 2.5 m in depth. Each tiltmeter is a double system, one filled with water, the other one with mercury, laid in parallel. The floaters and devices supporting the LVDT sensor measuring the liquid level are in silicium, and the containers are in pyrex. The latter are installed on granite tables, each supported by one granite column, 1.5 m long, anchored within the hard rock at 4 m in depth. The connecting tubes are in teflon for the water system, and in pyrex for the mercury. Evaporation of the liquids is inhibited by a layer of silicone oil. Protection against atmospheric perturbation is brought by a stack of polystyrene cubes on a layer of sand bags. The instrument is described in more details in Bernard et al. (2004) and Boudin (2004). It is operational with its present resolution since June 2003.

The short period tilt noise (minutes to hours) is higher on the water system than on the mercury by a factor about 10, and is mostly related to pressure perturbations due to wind: the higher density of the mercury strongly reduces this effect. The east component of the long base mercury tiltmeter shows a clear semi-diurnal tidal signal (amplitude 2×10^{-7} rad), whereas the north component shows a larger diurnal signal (8×10^{-7} rad) (Fig. 13). The short base tiltmeters (silicium penduli, *Blum* type, Blum et al. (1991)) installed in the same shelters present a similar behaviour, but the diurnal signal on the NS component is 1.8×10^{-6} rad. This leads us to interpret the diurnal signal as a thermostress effect at a scale of a few tens of meters to one hundred meters, related to the daily tilt of the local east–west trending hill on which the site is built. At periods ranging from minutes to hours, the rms noise level is a few 10^{-9} on the mercury tiltmeter. At the time of the December 3, 2002 transient, the rms noise

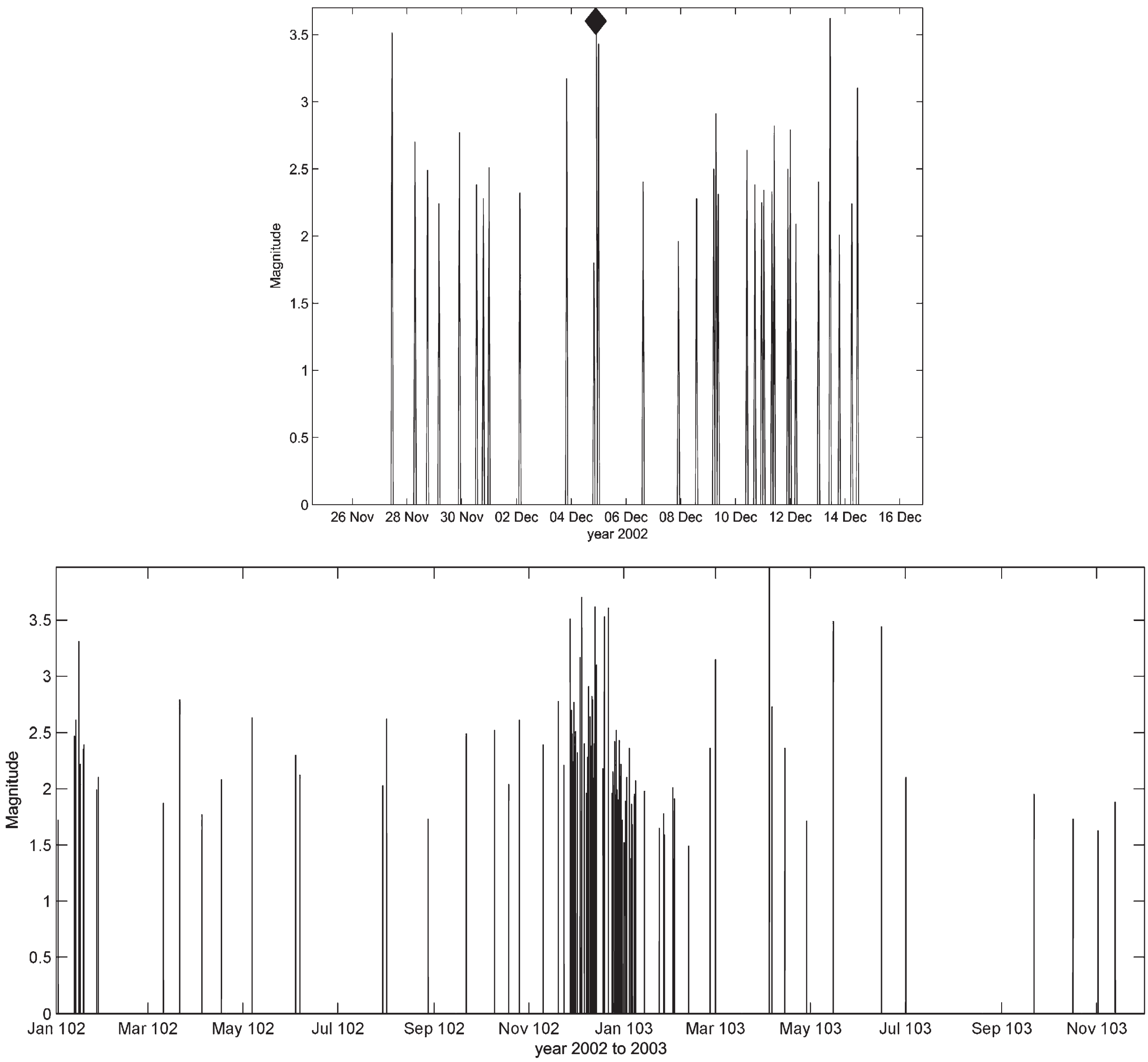

Fig. 12. Time sequence of the December 2002 swarm, from Patras University. Bottom: January 2002 to November 2003. Top: 25 November to 17 December 2002. The solid diamond is for the 2002, 3rd December earthquake coincident with the strain transient (Fig. 16). The selected earthquakes have epicenters less than 3′ latitude and longitude away from this event.

level was around 2×10^{-8}. As no signal is recorded, the deep source of this transient must have generated a tilt lower than 2×10^{-8} at Trizonia.

The underground shelter and trenches were prepared a year before installation, and the granite columns were in place in spring 2002, so that the mechanical relaxation of the site was probably mostly achieved by October 2002. Since November 2002, the tilt present a yearly component (Fig. 14). Its amplitude is 20×10^{-6} and 70×10^{-6} rad on the EW and NS directions respectively. This large difference between EW and NS rules out an explanation in terms of a direct effect of temperature on the sensors. A first interpretation could be a thermostress response, already revealed at shorter periods (Fig. 13). Another explanation could be the yearly cycle of groundwater loading. The stronger signal on the NS component may be due to a topographic low, whose center is located about 30 m south to the central vault. This depression collects water from the southern hill slope, mostly from November to April, which produces water table fluctuations of the order of 1 m. This in turn should generate a direct

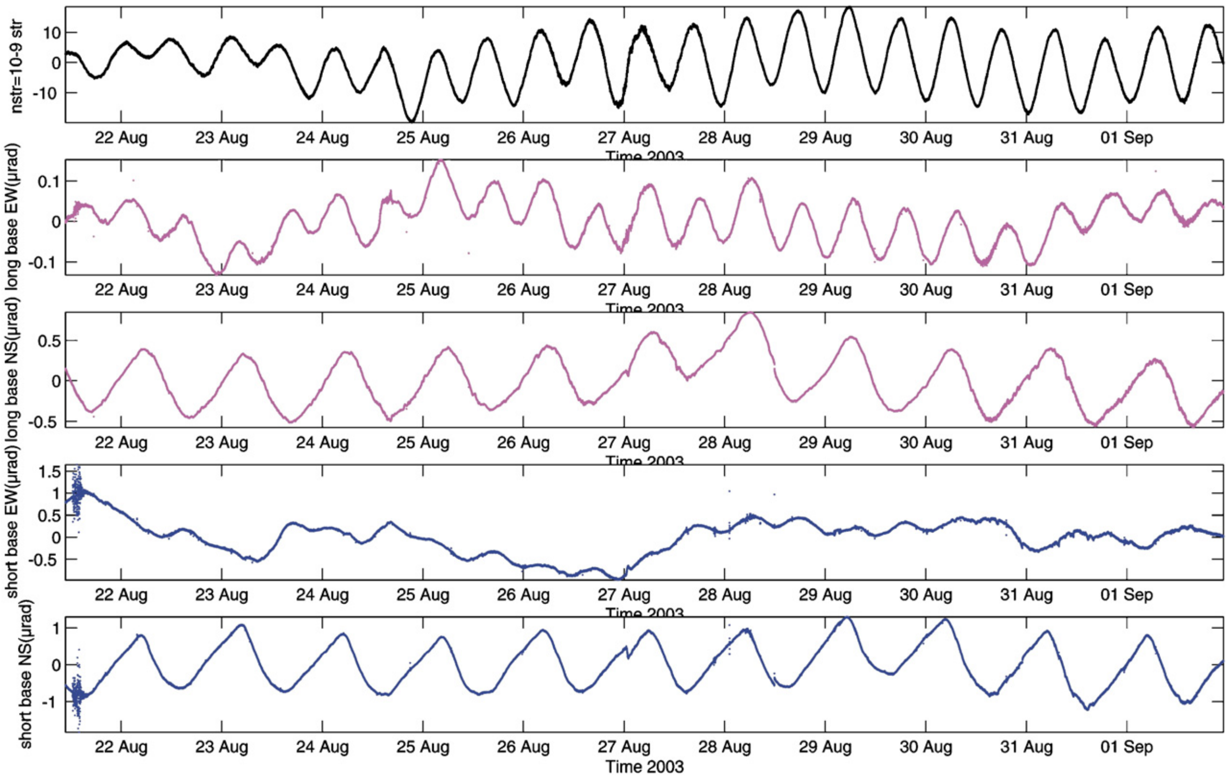

Fig. 13. Eleven days of tilt and strain records in Trizonia. From top to bottom: compression on the Sacks-Evertson dilatometer; EW tilt on the mercury tiltmeter; NS tilt on the mercury tiltmeter; EW tilt on the short-base Blum pendulum; NS tilt on the short-base Blum pendulum.

mechanical load and tilt, but also should saturate the radiolarite at the bottom of the southern vault (southern extremity of the NS level), and uplift its basis. The predicted sense of tilt, towards north in winter time, is indeed the one observed.

Removing the yearly cycle provides an estimate of the long term drift during the first year: $20\pm5\ 10^{-6}$ rad towards south, and $1\pm1\ 10^{-6}$ rad towards West. The drift of the NS component is too large to be accounted for by the secular tectonic loading, which is of the order of 10^{-6}. Most of this drift is thus likely to be due to the post-installation relaxation, which may die out in the coming years. Several years of recording are necessary to analyze the long term stability of the site.

6. AIG10: pore pressure at 1 km in depth

The AIG10 borehole has been drilled in 2002, in the Aigion harbour, down to 1000 m (DGLab-Corinth project) (Cornet et al., 2004b) (Fig. 15). It cuts the Aigion active normal fault at the depth of about 760 m, constraining its mean dip angle at $60°+-2°$. Geophysical investigations in the area and within the borehole, and the analysis of cores from the fault zone and above, has allowed to provide a first order model of the borehole geological and geophysical setting (Daniel et al., 2004; Naville et al., 2004).

These studies have revealed a 150 m of total cumulative displacement of the fault. The fault zone consists of an impermeable layer of clay, 0.5 m thick at the borehole crossing, dividing the karstic limestone body (Olonos-Pindos Nappe) into two compartments with a 0.5 MPa pore pressure difference. This clay, identified as radiolarite (and not fault gouge) (Sulem et al., 2004), is likely to result from the smearing of a bed within the fault zone due to its 150 m offset. As the hanging-wall limestones present an overpressure of 0.5 MPa, the total overpressure in the footwall limestone reaches about 1 MPa below 800 m. At greater depths, below the impermeable layer, the two limestone walls may be in direct contact on the fault, but nothing can be inferred on the permeability of the latter from the drilling observation.

A compound instrument consisting of seismometers, accelerometers, dynamic and static piezometers, tiltmeters, and temperature, has been designed for permanent installation at various depths in the borehole, above and below the fault zone. Its aim is to monitor the hydromechanical coupling on and near the fault zone,

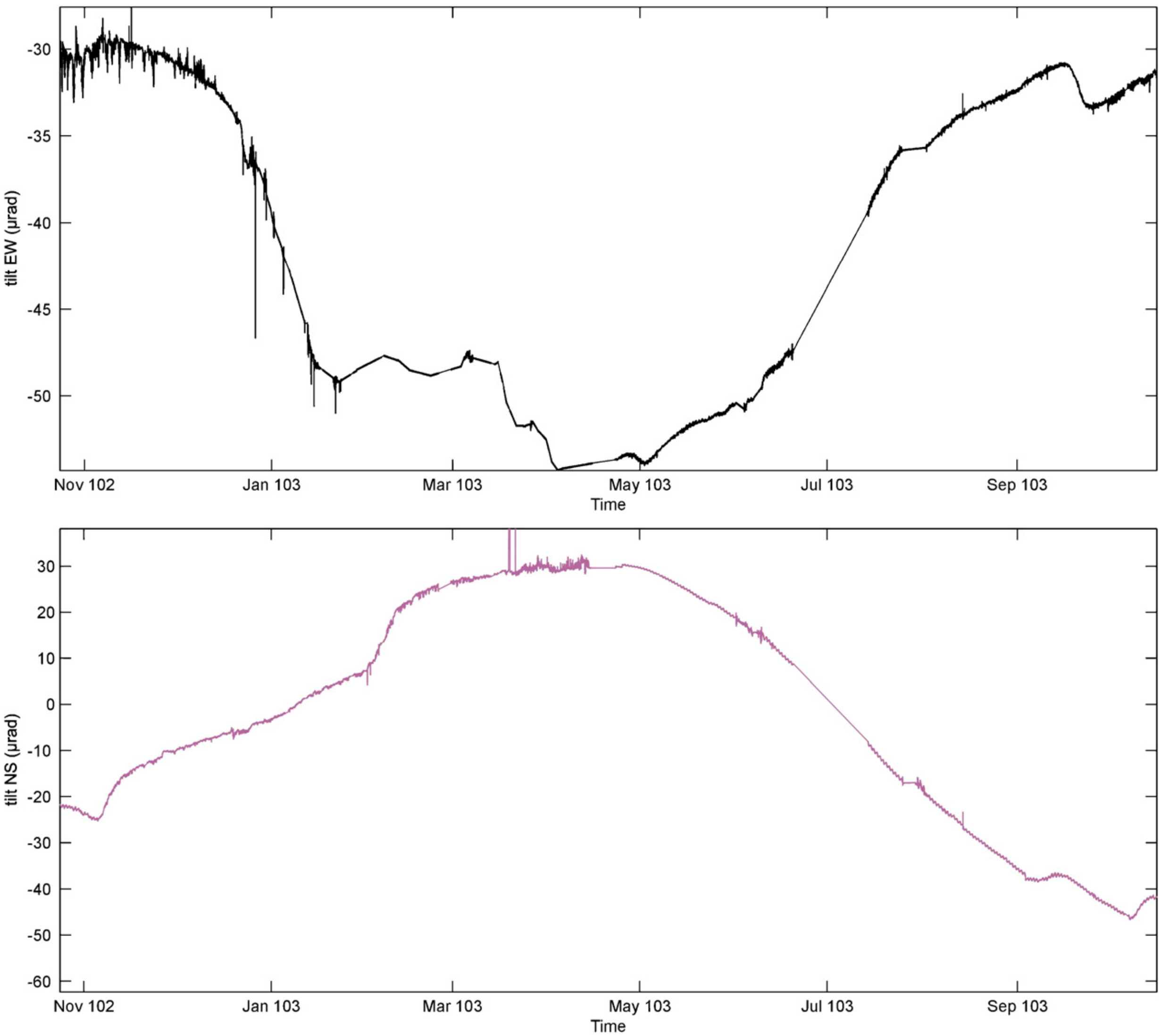

Fig. 14. Long term tilt in Trizonia. One year of tilt on the long base, EW water, positive towards east (top) and NS mercury, positive towards north (bottom) tiltmeters. The spikes on the water tiltmeter (until February) are related to the wind sensitivity, which has been reduced by an instrumental modification in April 2003. The 10 days period perturbations may be related to groundwater loading following heavy rain.

and in particular to bring *in situ* data revealing flow and creep transients. The first downhole installation was attempted in November 2003, but failed, as the instrument could not be downloaded due to an unexpectedly strong upward water flow in the borehole (450 m^3/h). The installation is now planned for spring 2007.

A piezometer was however installed in the borehole, near the surface, below the closing packer maintaining the overpressure. Its record shows a great sensitivity to strain, as evidenced by the level of tidal signal, reaching 0.03 bars, and by the clear record of long period waves from teleseismic earthquakes. As an example, Fig. 16 presents the record of the 25 September 2003 Hokkaido event. Note the absence of pressure signal for the P wave, due to its higher frequency content, and the strong signal associated to the S arrival, due to the S to P conversion at the surface. The achieved high resolution in strain reflects the large size and confined character of the karstic reservoir.

7. Discussion: fault geometry and activity at depth

The proposed geometry of the north-dipping Aigion and offshore faults, steep down to 6 km (60°), joining the low dip (10 ± 5°) seismic layer, has to be compared to the geometry of the fault located just to the east, which

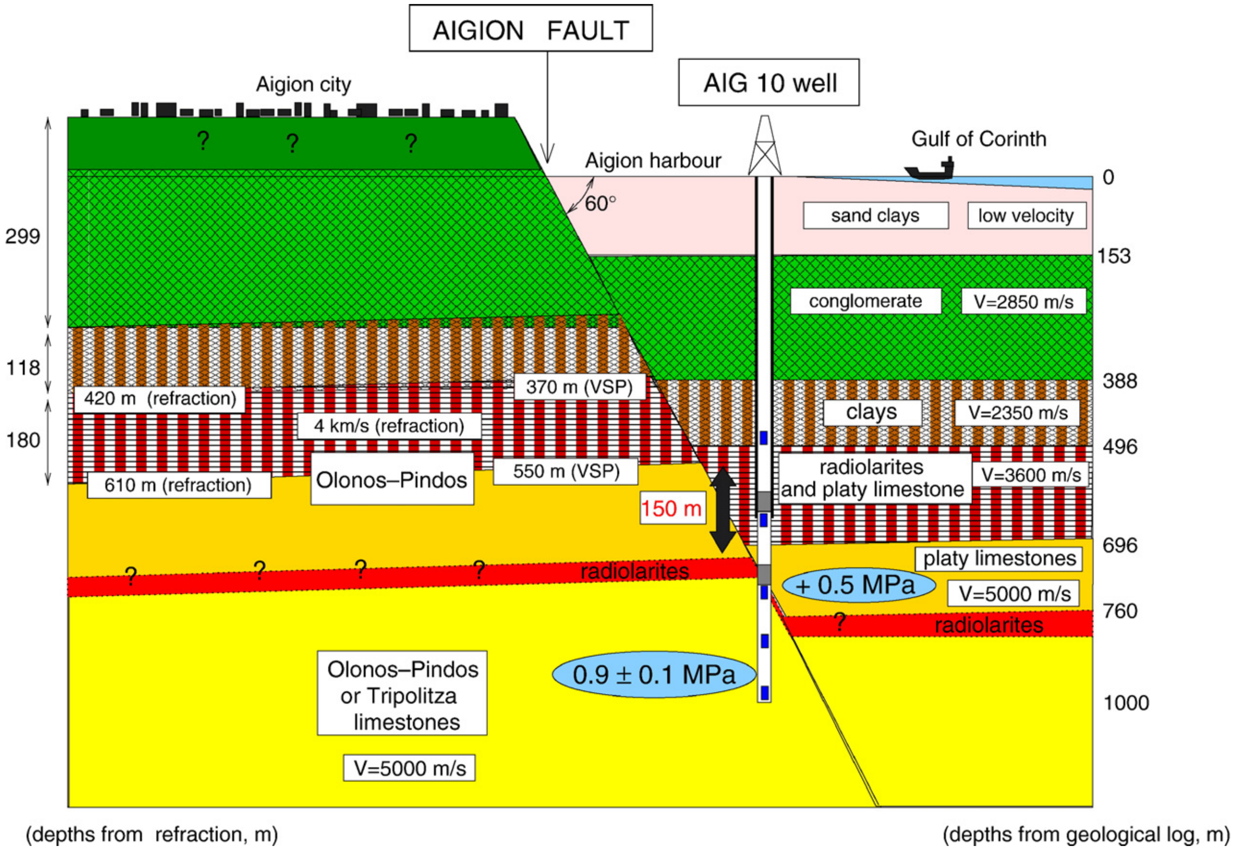

Fig. 15. Schematic cross-section of AIG10 borehole on the Aigion fault (from Cornet et al., 2004b).

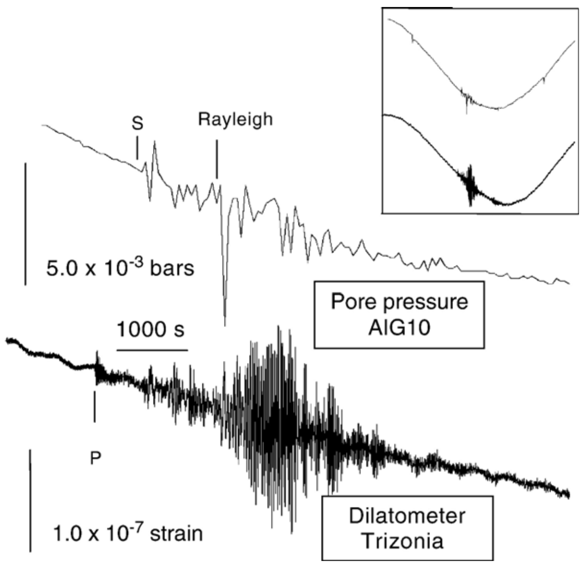

Fig. 16. Records of the Hokkaido 2003 earthquake on the pore pressure sensor of AIG10 (top) (from Cornet et al., 2004b), and borehole dilatometer of Trizonia (bottom). Top right insert: 12 h of both records.

ruptured in 1995 during the Aigion earthquake. The latter had a dip angle 30 to 35°, towards north, from 3–4 km to about 10 km in depth (Bernard et al., 1997). Thus, these geometries do not match at the fault boundaries. Furthermore, the inferred 60° dip of the offshore fault also differs from the low dip angle of the shallow active faults revealed in the first 4 km by active seismics, more to the east, in the central section of the rift (Clement et al., 2004).

Going west, the longitude at which this change in dip occurs (around 22°10′) corresponds to a 5 km *en echelon* step towards north of the antithetic offshore fault system, and to a clear narrowing of the rift (see Fig. 3). The dip change and fault step may thus both have the same structural control from pre-existing structures of the upper crust.

The shallow dipping layer in which the microseismicity is clustered is about 1.5±0.5 km thick. The low dip angle, single detachment fault plane proposed by Sorel (2000) cannot be associated with this seismicity, as this detatchment would be located several kilometers above the seismic layer. The top of this layer coincides with a strong vertical gradient in P wave velocity, as shown by a seismic 3D tomography with the records of the 1991 experiment (Latorre et al., 2004). Between 6 and 10 km in depth, this tomography also reveals a nearly horizontal layer with a high Vp/Vs ratio (around 2.0), extending towards north about 20 km from the root of the Helike and Aigion faults: this thick layer thus includes most of the reported microseismicity.

This seismic layer may correspond to a rheological change, either due to a pre-existing, low dip structure such as the hypothetical Phyllade nappe, as proposed by Le Pourhiet et al. (2004), or due to the shear localization processes itself, as proposed by Gueydan et al. (2003). In the former model, the drastic change to the east of Aigion (no clear microseismicity layer, low-dip angle for the major fault) could then be due to a significant change in the geometry of the Phyllade nappe — or even to its absence.

Finally, one should note that this microseismicity band is located 4 to 6 km above the highly conductive layer evidenced by MT sounding at 12 km in depth (Pham et al., 2000). The latter is thus clearly distinct from the seismic layer, and may be related to the top of the brittle–ductile transition at mid-crustal depth.

8. Discussion: seismic hazard in the western rift

The kinematic model of the rift extension deduced from the combination of GPS data and of microearthquake hypocentral locations can be used to constrain the probability of near-future, destructive earthquakes.

We assume here that the 15 mm/year of loading creep on the 15° dipping detachment zone are reported to and shared between the West Helike, the Aigion, the offshore and the Trizonia faults, with a total fault slip rate of 2 cm/year (taking into account the dip angle). We investigate three scenarios, varying the balance of the southern and northern fault activity, as detailed in Table 1, column 8 to 10. In scenario S1, the Helike and Aigion fault dominate the slip contribution. In scenario S2, all four faults have equal slip rate. In scenario S3, the offshore fault dominates the slip rate. More to the west, Table 1 takes the Kamarai fault slip rate at 5 mm/year, and the Psathopyrgos slip rate at 6 mm/year, for reasons which will be discussed later. When the fault slip cannot be directly estimated, we consider a coseismic fault slip to fault length ratio ranging between 0.3×10^{-4} to 1×10^{-4} (corresponding to standard stress drop range of a few MPa). This range agrees with the estimates for the Corinth 1981 and the Aigion 1995 events, with similar tectonic and structural environment: the slip to length ratio is about 0.7×10^{-4}, 0.2×10^{-4}, and 0.1×10^{-4} for the 1981 events (Jackson et al., 1982), and 0.6×10^{-4} for the 1995 earthquake (Bernard et al., 1997), leading to a mean value of 0.4×10^{-4}.

The Helike fault can be divided into three segments with different seismic potential. The eastern Helike fault was ruptured in 1861 by a large earthquake producing 1 m

Table 1

Fault	West Helike	Aigion	Offshore	Trizonia	Kamarai	Psathopyrgos
Length (km)	12±1	10±1	10±2	13±5	9±2	15±2
Width (km)	12±2	10±2	6±2	6±1	7±1	9±2
Slip (m), with $\Delta u/L=0.3–1\times10^{-4}$	0.31–1.30	0.27–1.10	0.24–1.20	0.24–1.80	0.21–1.10	0.39–1.70
Moment (10^{18} N m)	1.02–7.09	0.58–5.35	0.23–3.45	0.29–6.8	0.26–2.9	1.06–9.53
Range of potential moment magnitude	5.94–6.50	5.77–6.35	5.50–6.29	5.57–6.48	5.53–6.24	5.95–6.58
Date of most recent Probable Historical EarthQuake (PHEQ) and	1888	1748 (H1) 1817 H2	1748 (H2) 1817 (H1)	1909 (H3) <1750 (H4)	<1750	1917: M<6
Minimal slip (m) for $M>6$	0.38–0.22	0.31–0.58	0.43–1.3	0.31–1.04	0.47–0.99	max. slip 0.22 – 0.46
Mean slip rate mm/year (S1)	10	4	3	3	5	6
Mean slip rate mm/year (S2)	5	5	5	5	5	6
Mean slip rate mm/year (S3)	3	5	7	5	5	6
Slip (m) and magnitude potential recovery since last PHEQ (S1)	1.16 m $M=6.6$	(H1) : 1.02 $M=6.3$ (H2): 0.80 $M=5.9$	(H2): 0.77 $M=5.9$ (H1): 0.56 $M=5.8$	(H3): 0.28 $M=5.6$ (H4): >0.76 $M>6.0$	1.27 $M=6.4$	1.0–1.52 $M=6–6.5$
Slip (m) and magnitude potential recovery since last PHEQ (S2)	0.58 m $M=6.1$	(H1): 1.28 $M=6.5$ (H2): 1.0 $M=6.3$	(H2): 1.28 $M=6.3$ (H1): 0.93 $M=6.0$	(H3): 0.47 $M=5.8$ (H4): >1.27 $M>6.2$	1.27 $M=6.4$	1.0–1.52 $M=6–6.5$
Slip (m) and magnitude potential recovery since last PHEQ (S3)	0.35 m $M=6$	(H1): 1.28 $M=6.5$ (H2): 1.0 $M=6.3$	(H2): 1.79 $M=6.5$ (H1): 1.31 $M=6.4$	(H3): 0.47 $M=5.8$ (H4): >1.27 $M>6.2$	1.27 $M=6.4$	1.0–1.52 $M=6–6.5$

surface ruptures (Schmidt, 1879) (Fig. 3). The 0.8 m slip of the 1995 Aigion earthquake, located to the ENE of Aigion, also released stresses on this eastern Helike fault segment.

The central (Fig. 3, *cc′*) and eastern part (Fig. 3, *bb′*) of the western Helike fault is 12±1 km long. It is seismically active at shallow depths, suggesting some small creep process extending from 8 km to about 4 km in depth, undetected by GPS. This creep becomes much larger at greater depth, with an almost complete relaxation through continuous slip from 15 km downdip (segment F1). Thus, the interseismic slip rate distribution is equivalent to a locked zone with 12±2 km in width. With the allowed slip-to-fault length ratio defined above, this would lead to a moment magnitude of 6.0 to 6.5, and a mean seismic slip of 0.3 to 1 m.

From the analysis of the catalogue Papazachos and Papazachou (1997), the only large historical earthquake of the last three centuries which might be associated to the rupture of the western Helike fault occurred in 1888 (star in Fig. 3). No surface rupture were reported, unlike for the 1861 earthquake on the eastern Helike fault. The mean slip may thus have been smaller, or the scarp may have remained undetected. The three scenarios S1 to S3 show that the potential slip and magnitude recovery since the most recent probable historical earthquake (in 1888) ranges 0.35–1.20 m, and 6 to 6.6, respectively. The western Helike segment may then be close to produce an event similar to the 1888 rupture, within a few decades.

The Aigion fault is 10±1 km long, and its width is 10±2 km down to the shallow dip creeping section (F1). Paleo-earthquakes discovered in several trenches by Pantosti et al. (2004a) revealed a maximal average recurrence interval of 320–640 years, and a surface slip ranging from 0.4 to 0.7 m. The latter involves moment magnitudes ranging from 5.8 to 6.2. The offshore fault, 3 km north to Aigion, has a similar size to that of the Aigion fault. Its long term activity may thus be similar. From the analysis of the catalogue of Papazachos and Papazachou (1997), for the last 3 centuries, the only historical, destructive earthquakes which are likely to have ruptured one or both of these faults occurred in 1748 and 1817, with estimated magnitudes around 6 (star in Fig. 3). They were both associated with large tsunamis (several meters). One may thus evaluate two alternative hypothesis, that the most recent significant earthquake on the Aigion fault was in 1748 (hypothesis H1) or in 1817 (hypothesis H2). Combined with the three scenarios S1 to S3, this provides six estimates of slip and magnitude potential recovery (Table 1): the slip ranging from 0.8 m to 1.3 m, and the magnitude from 5.9 to 6.5. Thus, the Aigion fault is also in a state close to rupture. The same arguments can be put for the offshore fault. Its smaller size (10±2 km×6±2 km) provides slightly smaller potential magnitudes (see Table 1).

In 1909, a destructive earthquake hit villages 10 to 20 km NE to the Trizonia island (Ambraseys and Jackson, 1990) (star in Fig. 3). It is unlikely to be associated to the main, north dipping faults, as their ruptures are expected to generate dominant damage on the southern coast, as was illustrated during the 1995 earthquake. The south-dipping Trizonia fault and/or its eastern continuation may be an acceptable candidate for this event. Its smaller width (7 km) may imply an earthquake with magnitude 6 or less. The slip and magnitude potential recovery since 1909 would then be 0.3 to 0.5 m, and 5.6 to 5.8, respectively (Table 1, H3). We may alternatively propose that this earthquake occurred on a hidden, rather shallow fault under the north coast. The cluster of seismic activity around 6 km in depth, north and east to the Trizonia island, may be related to such a structure, and thus deserves refined studies. In this case, the slip and magnitude potential recovery of the Trizonia fault are greater than 0.8 m and 6.0, respectively (Table 1, H4).

The Psathopyrgos fault, to the west, 15±2 km long, is poorly documented by the present seismic array, except in its easternmost part. There, the microseismicity location suggests a steep dip angle (50 to 60°) of the fault, and a fault width of 9±2 km. Earthquakes with magnitude 6 to 6.6 could be expected on this fault, with characteristic slip of 0.4 to 1.7 m (Table 1). No large earthquake have occurred on this fault during the last 3 centuries, except possibly the 1917 event. The latter however produced significant damage only near Nafpaktos (Papazachos and Papazachou, 1997), on the northern coast, above the NW edge of the fault. It is thus unlikely to have ruptured the whole fault up to the surface on the southern coast, which is supported by the absence of tsunami report. Neglecting the contribution of this event (less than 0.5 m slip), one gets a missing slip of at least 4.5 to 6 m if one takes a minimal 15 mm/year slip rate inferred from GPS. As these values are much too large for a normal faulting slip (one would expect at most 2 m) (see for instance Wells and Coppersmith, 1994), one is lead to propose that the present extension rate be seen by GPS is an accelerated state, near the end of the seismic cycle. Assuming a mean extension rate of 5 mm/year, one third to half of the present day value at this location, one still gets more than 1.5 to 2 m of missing slip, which can be considered as close to an upper limit of a sustainable strain. Thus, one may suggest that not only the present slip rate, about

15 mm/year averaged since 1990, is two to three times the average interseismic value, but also that the considered faults are close to their failure time, within a few decades. The slip and magnitude potential recovery of this fault is calculated for 6 mm/year in Table 1, leading to 1 to 1.5 m, and 6 to 6.5, respectively.

The *en echelon* Kamarai normal fault connecting the Aigion fault to the Psathopyrgos fault is a young structure at the surface, and would thus be expected to have relatively low slip rates. However, it seems to significantly control the microseismicity on the detachment surface at 6 to 8 km in depth. This suggests that it is already well developed at depth. It is about 9±2 km long and 7±1 km wide, which provides potential for a magnitude 5.6 to 6.2. It also can significantly participate to the rupture of the nearby, larger segments, increasing their potential magnitude. The simultaneous slip of this fault, to its east with that of the Aigion or offshore fault, or to its west with the Psathopyrgos fault, makes the potential for a magnitude 6.2 to 6.7 earthquake. It may have ruptured in such a way, with the Aigion fault, in 1748 or 1817. If it did not break in historical times (since the 18th century), its slip and magnitude potential recovery would be larger than 1.3 m and 6.4, respectively, assuming a 5 mm/year slip rate (Table 1). Larger slip rate values would imply a present unreasonable slip potential, as for the Psathopyrgos fault, and this part of the rift might also be in a state of recently accelerated slip.

In conclusion of this hazard analysis, one shall say that all the major north dipping fault segments identified in the area are in the late part of their seismic cycle, each of them being able to generate a magnitude 6 to 6.5 earthquake, possibly up to 6.7 (6.9) if two (three) are activated in a single dynamic rupture. Among these faults, the western Helike fault and the Aigion faults present microseismic activity as shallow as 5 km and 3.5 km in depth, respectively, suggesting partial seismic creep on most of their surface. This creep is however not resolved by GPS, and may range from 0 to about 10 mm/year. This should deserve a particular attention, as it may diagnose the start of the frictional destabilization process of these two faults. Finally, our hypothesis of a transient accelerated strain rate to the west needs to be tested through an improved instrumentation with additional seismometer and GPS sites.

In terms of seismic risk, it is important to note that although the same earthquake magnitude can be achieved by the rupture of the Trizonia fault and by that of the Aigion (or Offshore) fault, both ruptures would strongly differ in the resulting damage. Indeed, the Aigion city is expected to suffer much more from the rupture of the north-dipping faults, due to directivity effects and fault proximity Thus, quantifying the statistical share of large earthquakes between these antithetic faults appears an important issue for seismic risk assessment.

In order to better quantify the above predictions, one will need refined strain measurements, non-elastic 3D strain modelling, a seismic catalogue covering a longer time period, and a refined knowledge of the crustal structure and fault locations through detailed passive and active seismic tomography.

9. Conclusion

Since a couple of years, the various monitoring arrays of CRL have produced new data allowing a better understanding of the seismicity and deformation pattern of the western rift of Corinth, and an improved assessment of the related seismic hazard.

Most of the microseismicity is confined in a band which is 1.5+0.5 km thick, gently dipping to the north, centered at about 6 km (resp. 8 km) in depth to the south (resp. north). The northern, deepest part of this seismic layer is continuously relaxing most of the rift extension rate. This layer could be due to the low viscosity expected from the plausible presence of the Phyllade Nappe at these depths (Le Pourhiet et al., 2004).

All active normal faults dip at large angles (50° to 60°) and root into this active layer, possibly extending further within it (see sketch in Fig. 5). This differs from the normal faults more to the east, which dip at smaller angles (30 to 35°) (Galaxidi 1992 and Aigion 1995 earthquakes), suggesting a major structural change, such as the possible absence of the Phyllade nappe to the east. The Aigion and Helike faults are associated with microseismicity at shallow depths, between 3.5 and 5 km. The Kamarai and Psathopyrgos faults are locked above 6 km in depth. The offshore faults, to the contrary, may sustain large creep in the last few kilometres. The western part of the West Helike fault shows no significant microseismic activity, in agreement with the absence of long term activity deduced for geological data. It is taken over to the north by the young Kamarai fault connecting the Aigion and Psathopyrgos faults. Our fault model with specific creeping segments, adjusted to the repeated GPS data, predicts a significant subsidence of the central part of the rift, which fits the 5 mm/year of subsidence at the continuous GPS site on the Trizonia island.

The roots of the Aigion, Kamarai, and Psathopyrgos faults within the seismicity layer at 5 to 7 km in depth mark the WNW-ESE trending limit between the high-seismicity and fast straining band to the north (15 mm/year), with a lower-seismicity, slowly straining band to the south. All of these faults, together with the offshore faults, are in the late part of their seismic cycle. The probability of at least one moderate to large earthquake (M=6.0 to 6.5) is thus very high within the next few decades. The possibility of cascade events – favoured by this large-scale "critical" state of the whole western fault system – should also be investigated, with the rupture of two or three fault segments at once with a magnitude ranging between 6.5 and 6.9.

The other new observations concern strain transients. Two recent seismic swarms may have involved a significant component of aseismic creep. The spring 2001 crisis, 5 to 8 km below the Helike fault trace, including several multiplets, has been produced by the reactivation of an old pre-rift fault (Lyon-Caen et al., 2004), possibly through seismic creep. The December 2002 crisis, located about 15 km west to Trizonia, was most probably related with a slow transient strain recorded on the Trizonia dilatometer with an equivalent magnitude 5±0.5. The newly installed pressiometer in the AIG10 borehole, and the tiltmeter in Trizonia now contribute to a denser array of high-resolution strain-gages, able to detect and constrain such transient processes. This array will be completed by a second borehole strainmeter in 2006.

Finally, the GPS and seismicity studies suggest the existence of a medium-term transient: the strain rate of the western part of the rift is at least twice the mean interseismic value, and may be significantly increasing at a time scale of a few decades. This acceleration could be diagnostic of a growing instability towards seismic rupture of the Psathopyrgos fault.

Acknowledgments

We are grateful to the two anonymous reviewers and to the Associate Editor whose comments and criticisms significantly improved the clarity, focussing, and consistency of the manuscript. This work was partially supported by the E.C. projects CORSEIS and 3HAZ-Corinth (contracts EVG1 CT99 00003 and GOCE 004043) and by the CNRS/GDR Corinth program. It would not have been possible without the active and efficient support of the local Greek authorities and population for the site installation and instrument operation.

References

Alexandri, N., Nomikou, P., Ballas, D., Lykousis, V., Sakellariou, D., 2003. Swath bathymetry map of Corinth Gulf. Geophys. Res. Abstr. 5, 14268 (EGS).

Ambraseys, N.N., Jackson, J.A., 1990. Seismicity and associated strain of central Greece between 1890 and 1988. Geophys. J. Int. 101, 663–708.

Armijo, R., Meyer, B., King, G., Rigo, A., Papanastassiou, D., 1996. Quaternary evolution of the Corinth rift and its implications for the late Cenozoic evolution of the Aegean. Geophys. J. Int. 126, 11–53.

Avallone, A., Briole, P., Agatza-Balodimou, A.M., Billiris, H., Charade, O., Mitsakaki, C., Nercessian, A., Papazissi, K., Paradissis, D., Veis, G., 2004. Analysis of eleven years of deformation measured by GPS in the Corinth Rift Laboratory area. C. R. Geosci. 336, 301–312.

Baker, C., Hatzfeld, D., Lyon-Caen, H., Papadimitriou, E., Rigo, A., 1997. Earthquake mechanisms of the Adriatic sea and western Greece. Geophys. J. Int. 131, 559–594.

Bernard, P., 2001. From the search of precursors to the research on crustal transients. Tectonophysics 338, 225232.

Bernard, P., Boudin, F., 2001. The CORSEIS subsurface geophysical array. Abstract, 1rst CRL Workshop, Aigion. 30 September 2001.

Bernard, Briole, P., Meyer, B., Lyon-Caen, H., Gomez, J.-M., Tiberi, C., Berge, C., Cattin, R., Hatzfeld, D., Lachet, C., Lebrun, B., Deschamps, A., Courboulex, F., Laroque, C., Rigo, A., Massonnet, D., Papadimitriou, P., Kassaras, J., Diagourtas, D., Makropoulos, K., Veis, G., Papazisi, E., Mitsakaki, C., Karakostas, V., Papadimitriou, P., Papanastassiou, D., Chouliaras, G., Stavrakakis, G., 1997. The Ms=6.2, June 15, 1995 Aigion earthquake (Greece): evidence for low angle normal faulting in the Corinth rift. J. Seismol. 1, 131–150.

Bernard, P., Pinettes, P., Bouin, M.-P., Gamar, F., Pham, V.N., Dubegny, C., Vandemeulebrouck, J., Gariel, J.-C., Robé, M.-C., Sabroux, J.-C., Richon, P., Labed, V., Abbad, S., Makropoulos, K., Tzanis, A., Papadimitriou, P., Diagourtas, D., Veis, G., Milas, Stavrakakis, G., Chouliaras, G., Scherbaum, G.F., Ducarme, B., Van Ruymbecke, M., 2000. GAIA: a European test site for earthquake precursors and crustal activity: the gulf of Corinth, Greece. In: Thorkelsson, B., Yeroyanni, M., Reykjavik, E.C. (Eds.), Proceedings 2nd EU-Japan Workshop on Seismic Risk, pp. 122–135. Iceland.

Bernard, P., Boudin, F., Sacks, S., Linde, A., Blum, P.-A., Courteille, C., Esnoult, M.-F., Castarded, H., Felekis, S., Billiris, H., 2004. Continuous strain and tilt monitoring on the Trizonia island, Rift of Corinth, Greece. C. R. Geosci. 336, 313–324.

Blum, P.A., Bordes, J.L., Goguel, B., Le Magouarou, A., 1991. Performances and applications of a very high resolution tiltmeter. Field Measurements in Geotechnics (Serum Ed.). Balkema Pub., Rotterdam, pp. 139–151.

Boudin, F. 2004. Développement d'un inclinomètre hydrostatique à double niveau, et application au Golfe de Corinthe, Grèce, PhD thesis, IPGP.

Briole, P., Rigo, A., Lyon-Caen, H., Ruegg, J.C., Papazissi, K., Mitsakaki, C., Balodimou, A., Veis, G., Hatzfeld, D., Deschamps, A., 2000. Active deformation of the Corinth rift, Greece: results from repeated Global Positioning System surveys between 1990 and 1995. J. Geophys. Res. 105, 25605–25625.

Clarke, P.J., Davies, R.R., England, P.C., Parsons, B.E., Billiris, H., Paradissis, D., Veis, G., Cross, P.A., Denys, P.H., Ashkenazi, V., Bingley, R., 1997. Geodetic estimation of seismic hazard in the Gulf of Corinth. Geophys. Res. Lett. 24, 1303–1306.

Clement, Ch., Sachpazi, M., Charvis, Ph., Graindorge, D., Laigle, M., Hirn, A., Zafiropoulos, G., 2004. Reflection–refraction seismics in the Gulf of Corinth: hints at deep structure and control of the deep marine basin. Tectonophysics (Amsterdam) 391, 85–95.

Cornet F.H., I. Vardoulakis, I. Moretti, P. Bernard and G. Borm, 2001; *Proceedings of the CRL Aigion Workshop*; accessible from www.corinth-rift-lab.org.

Cornet, F.H., Bernard, P., Moretti, I., 2004a. On the Corinth rift problematic and the special Geoscience issue. C. R. Geosci. 336, 235–242.

Cornet, F.H., Doan, M.L., Moretti, I., Borm, G., 2004b. Drilling through the active Aigion fault: the AIG10 well observatory. C. R. Geosci. 336, 395–406.

Daniel, J.-M., Moretti, I., Micarelli, L., Essautier Chuyne, S., Delle Piane, C., 2004. Macroscopic structural analysis of AG10 well (Gulf of Corinth). C. R. Geosci. 336, 435–444.

Dragert, H., Wang, K., James, T.S., 2001. A silent slip event on the deeper Cascadia subduction interface. Science 292, 1525–1528.

Flotté, N., 2003. Caractérisation structurale et cinématique d'un rift sur détachement: le rift de Corinthe — Patras, Grèce, *Ph.D. Thesis, Univ. Paris XI*.

Ghisetti, F., Vezzani, L., 2004. Plio-pleistocene sedimentation and fault segmentation in the Gulf of Corinth (Greece) controlled by inherited structural fabric. C. R. Geosci. 336, 243–250.

Gueydan, F., Leroy, Y., Jolivet, L., Agard, P., 2003. Analysis of continental midcrustal strain localization induced by microfracturing and reaction-softening. J. Geophys. Res. 108 (B2), 2064, doi:10.1029/2001JB000611.

Hatzfeld, D., Kementzetzidou, D., Karakostas, V., Ziazia, M., Nothard, S., Diagourtas, D., Deschamps, A., Karakaisis, G., Papadimitriou, P., Scordilis, M., Smith, R., Voulgaris, N., Kiratzi, S., Makropoulos, K., Bouin, M.-P., Bernard, P., 1996. The Galaxidi earthquake of 18 November, 1992: a possible asperity within the normal fault system of the Gulf of Corinth (Greece). Bull. Seismol. Soc. Am. 86, 1987–1991.

Hatzfeld, D., Karakostas, V., Ziazia, M., Kassaras, I., Papadimitriou, E., Makropoulos, K., Voulgaris, N., Papaioannou, C., 2000. Microseismicity and faulting geometry in the Gulf of Corinth (Greece). Geophys. J. Int. 141, 438–456.

Herring, T., 1998. Documentation for GLOBK: Global Kalman filter for VLBI and GPS analysis program, version 4.1. Massachusetts Institute of Technology, Cambridge, MA.

Jackson, J., Gagnepain, J., Houseman, G., King, G.C.P., Papadimitriou, P., Soufleris, C., Virieux, J., 1982. Seismicity, normal faulting and the geomorphological development of the Gulf of Corinth (Greece): the Corinth earthquakes of February and March 1981. Earth Planet. Sci. Lett. 57, 377–397.

King, R.W., Bock, Y., 1998. Documentation for the GAMIT Analysis Software, Release 9.7. Massachusetts Institute of Technology, Cambridge, MA.

Latorre, D., Virieux, J., Monfret, T., Monteiller, V., Vanorio, T., Got, J.-L., Lyon-Caen, H., 2004. A new seismic tomography of Aigion area (Gulf of Corinth, Greece) from the 1991 data set. Geophys. J. Int. 159, 1013–1031.

Léonardi, V., Gavrilenko, P., 2004. Hydrologic measurements in wells in the Aigion area (Corinth Gulf, Greece): preliminary results. C. R. Geosci. 336, 385–394.

Le Pourhiet, L., Burov, E., Moretti, I., 2004. Rifting through a stack of inhomogeneous thrusts (the dipping pie concept). Tectonics 23, TC4005, doi:10.1029/2003TC001584.

Linde, A., Gladwin, T.M., Johnston, M.J.S., Gwyhter, R.L., Bilham, R.G., 1996. A slow earthquake sequence on the San Andreas fault. Nature 383, 65–68.

Lyon-Caen, H., Papadimitriou, P., Deschamps, A., Bernard, P., Makropoulos, K., Pacchiani, F., Patau, G., 2004. First results of the CRLN seismic network in the western Corinth rift: evidence for old fault reactivation. C. R. Geosci. 336, 343–352.

Makropoulos, K., Drakopoulos, J., Latousakis, J., 1989. A revised and extented earthquake cataloque for Greece since 1900. Geophys. J. Int. 98, 391–394.

Moretti, I., Sakellariou, D., Lykousis, V., Micarelli, L., 2003. The Gulf of Corinth: a half graben? J. Geodyn. 36, 323–340.

Naville, Ch., Serbutoviez, S., Moretti, I., Daniel, J.-M., Throo, A., Girard, F., et al., 2004. Pre-drill surface seismic in the vicinity of the AIG-10 well and post-drill VSP. C. R. Geosci. 336 (4–5), 407–414.

Okada, Y., 1992. Internal deformation due to shear and tensile faults in a half-space. Bull. Seismol. Soc. Am. 82, 1 0181 040.

Pacchiani, F., Lyon-Caen, H., Bourouis, S., Bernard, P., Deschamps, A., Papdimitriou, P., Makropoulos, K., 2003. Relocation of the microseismicity in the Corinth rift and implications on the faulting geometry, abstract, EGU.

Pantosti, D., De Martini, M., Koukouvelas, I., Stamatopoulos, L., Palyvos, N., Pucci, S., Lemeille, F., Pavlides, S., 2004a. Paleoseismological investigations of the Aigion fault (Gulf of Corinth, Greece). C. R. Geosci. 336, 335–342.

Pantosti, D., Palyvos, N. (eds), Eliki and Aigion fault GIS data base, E.C. 2004b. CORSEIS project http://www.ingv.it/~wwwpaleo/pantosti/aigion/database.

Papazachos, B., Papazachou, K., 1997. The Earthquakes in Greece, Ed. Ziti.

Pham, V.N., Bernard, P., Boyer, D., Chouliaras, G., Le Mouël, J.-L., Stavrakakis, G.N., 2000. Electrical conductivity and crustal structure beneath the central Hellenides around the Gulf of Corinth (Greece) and their relationship with the seismotectonics. Geophys. J. Int. 142, 948–969.

Pinettes, P., Précurseurs géophysiques des séismes: Approches expérimentales et modélisations; *Ph. D. thesis*, Univ. Paris 7, Paris 1997 (in French).

Pinettes, P., Bernard, P., Blum, P.-A., Verhille, R., Milas, P., Veis, G., 1998. Strain constraint on the source of the alledged VAN precursor of the 1995 Aigion earthquake (Greece). J. Geophys. Res. 103, 15145–15155.

Pitilakis, K., Makropoulos, K., Bernard, P., Lemeille, F., Berge-thierry, C., Tika, Th., Manakou, M., Diagourtas, D., Raptakis, D., Kallioglou, P., Makra, K., Pitilakis, D., Bonilla, L.F., 2004. The Corinth gulf soft soil array (CORSSA) to study site effects. C. R. Geosci. 336, 353–366.

Pizzino, L., Quattrocchi, F., Cinti, D., Galli, G. 2004. Fluid Geochemistry along the Eliki and Aigion seismogenic segments (Gulf of Corinth, Greece). *C. R. Geosciences*, 336, 367–374.

Rigo, A., Lyon-Caen, H., Armijo, H.R., Deschamps, A., Hatzfeld, D., Makropoulos, K., Papadimitriou, P., Kassaras, I., 1996. A microseismic study in the western part of the Gulf of Corinth (Greece): implications for large scale normal faulting mechanisms. Geophys. J. Int. 126, 663–688.

Sacks, I.S., Suyehiro, S., Evertson, D.W., Yamagishi, Y., 1971. Sacks-Evertson strainmeter, its installation in Japan and some preliminary results concerning strain steps. Pap. Meteorol. Geophys. 22, 195–208.

Sakellariou, D., Lykousis, V., Moretti, I., Kaberi, H., 2003. Late quaternary evolution of the cental Gulf of Corinth basin, abstract, CRL workshop, Aigion. June 2.

Schmidt, J., 1879. Studien uber Erdbeben. Carl Schottze, Leipzig, pp. 68–83.

Sorel, D., 2000. A Pleistocene and still active detachment fault ad the origin of the Corinth Patras rift, Greece. Geology 28, 80–86.

Sulem, J. (1), Vardoulakis, I., Ouffroukh, H. (1), Boulon, C.R. (3) J.M. Hans (3). 2004.Experimental characterization of the thermo-poro-mechanical behaviour of the Aegion fault gouge, *Geosciences*, 336, 455–466.

Wells, D.L., Coppersmith, K.J., 1994. New empirical relationships among magnitude, rupture length, rupture width, rupture area, and surface displacement. Bull. Seismol. Soc. Am. 84, 974–1002.

Zahradnik, J., 2003. Three BB + SM seismic stations in the Corinth Gulf, jointly operated by the universities in Prague and Patras, abstract, 2nd CRL workshop, Aigion. June 2.

Zahradnik, J., Jansky, J., Sokos, E., Serpetsidaki, A., Lyon-Caen, H., Papadimitriou, P., 2004. Modeling the ML = 4.7 mainshock of the February–July 2001 earthquake sequence in Aegion, Greece. J. Seismol. 8, 246–257.

Zlotnicki, J., Kanwar, R., Le Mouël, J.L., Yvetot, P., Vargemezis, G., Menny, P., Fauquet, F., 2005. Ground-based electromagnetic studies combined with remote sensing based on Demeter mission: a way to monitor Corinth rift zone (Greece), abstract, IAGA.